POLITECNICO DI MILANO

Dipartimento di Energia

DEVELOPMENT AND VALIDATION OF A NEW NEUTRONIC MODEL OF THE TRIGA MARK II REACTOR

Relatore: Prof. Antonio Cammi
Correlatore: Christian Castagna

Tesi di laurea di:
Carlotta Giuliana Ghezzi Matr. 882974

Anno accademico 2018/2019

Ringraziamenti

Alla mia mamma e al mio babbo.

Sommario

Il presente lavoro di tesi ha come obiettivo lo sviluppo e la validazione di un modello neutronico del reattore TRIGA Mark II dell'Università di Pavia, aggiornato all'ultima configurazione di criticità risalente al 2013. Il codice ottenuto si basa su un modello sviluppato in precedenza con il codice Monte Carlo Serpent e relativo alla configurazione originale del reattore datata 1965, la quale è cambiata negli anni e i materiali hanno subito fenomeni di burnup. In questo lavoro, il modello è stato aggiornato all'ultima configurazione di criticità, in modo da avere un codice nuovo e utilizzabile come strumento di analisi del reattore per le attuali condizioni operative dell'impianto. I dati utilizzati per aggiornare il modello sono relativi alla configurazione del nocciolo ottenuta a settembre 2013 e sono stati sfruttati calcoli di burnup effettuati tramite precedenti analisi e relativi allo stesso arco temporale. La verifica e validazione per il modello sviluppato sono stata effettuate rispettivamente tramite confronto code-to-code con un modello MCNP e analisi di benchmark con i dati sperimentali sia per le criticità a diversi livelli di potenza, sia per il core excess. In entrambi i casi si sono ottenuti risultati compatibili con i dati sperimentali. Si è successivamente simulata la calibrazione di due barre di controllo, da sottoporre ad analisi di benchmark con i dati sperimentali relativi agli anni 2015 e 2018. Per quanto riguarda il 2015, Serpent presenta risultati in accordo con i dati sperimentali, conclusione che si può trarre anche per i dati relativi al 2018. Simulazioni relative alle configurazioni di criticità per entrambi gli anni mostrano risultati in accordo con i dati sperimentali, nonostante per il 2018 vi siano livelli di reattività più elevati, ma comunque accettabili se si considerano errori di tipo sistematico di cui si ha una stima in termini di limite inferiore proveniente da lavori precedenti. Risulta quindi possibile affermare che il modello aggiornato rappresenta fedelmente le condizioni del reattore ed è un utile strumento di analisi dello stesso.

Abstract

This thesis work discusses the development and validation of an updated neutronics model for the reactor TRIGA Mark II of the University of Pavia. This work finds its basis on a preceding model developed in the past with the Monte Carlo code Serpent and based on the reactor fresh fuel configuration. The model has been adapted in order to be as close as possible to reactor present conditions and, for this purpose, data coming from MCNP burnup calculations up to September 2013 and a new core configuration regarding the same year have been employed and implemented in Serpent-compatible input files. The updated model underwent a code-to-code comparison to MCNP for the first full power criticality configuration and for the core excess simulation. For these same cases a validation via a benchmark analysis with experimental data was performed as well. In both circumstances the results were in good agreement with experimental data. The model was then employed to calibrate two control rods. Two datasets were exploited to compare simulation results, one collected in 2015 and one collected in 2018. The results obtained through Serpent appeared to be in good agreement with experimental data for what concerns the 2015 experimental data; this can be stated for results pertaining 2018 as well. Simulations regarding criticality configurations for both datasets were run as well, obtaining results compatible in both cases with experimental ones, even though reactivity values for the year 2018 resulted in being slightly higher. Despite this last consideration, all criticality simulations outputs resulted in being acceptable if considering systematic uncertainties, whose minimum value had been quantified with previous studies. In conclusion, the updated model can be defined as a valid reactor analysis tool.

Estratto in italiano

Introduzione

Negli ultimi anni, a seguito dello sviluppo che ha caratterizzato i sistemi di calcolo, l'analisi di sistemi quali i reattori nucleari si è sempre di più appoggiata all'utilizzo di simulazioni basate su modelli atti a riprodurre i suddetti impianti. Il vantaggio di queste ultime è legato sia ad una sensibile riduzione delle tempistiche computazionali, sia alla possibilità di esplorare in maniera esaustiva diversi lati e caratteristiche legati ad un determinato fenomeno. Esse permettono, da un lato, di evitare i costi legati all'installazione di impianti sperimentali e, dall'altro, di studiare e caratterizzare con maggiore accuratezza gli aspetti fenomenologici del reattore, visto come sistema multi-fisico. Il reattore costituisce un sistema la cui analisi abbraccia diverse branche, come quelle della termomeccanica, termoidraulica e neutronica. In particolare, in questo lavoro, l'aspetto cui si è rivolta attenzione è quello legato alla neutronica. Uno strumento altrettanto valido per la verifica e validazione dei sopra citati modelli è rappresentato dai reattori di ricerca, come il reattore TRIGA Mark II dell'Università di Pavia, già utilizzato in passato a questi scopi. Il lavoro qui presentato ha come scopo lo sviluppo e validazione di un modello tramite il codice Monte Carlo Serpent per il reattore TRIGA Mark II dell'Università di Pavia, caratterizzato dalla configurazione attuale del reattore, il cui ultimo aggiornamento risale al 2013. L'utilizzo di tale modello è volto all'applicazione dello stesso come strumento di analisi per le condizioni operative attuali del reattore. La base di partenza per il lavoro è stato un modello riferito alla configurazione a combustibile fresco del reattore (1965 circa) sviluppato con una precedente versione di Serpent (Castagna et al, 2017), da adattare all'attuale versione di Serpent che viene utilizzata e da aggiornare con dati riferiti alle composizioni e densità dei materiali all'intero del reattore riferiti al 2013. Gli

strumenti disponibili per la validazione del modello sono dati, sia sperimentali sia ottenuti tramite altri codici Monte Carlo, relativi a grandezze quali il *core excess* e alcune configurazioni di criticità. In ultima analisi di validazione sono disponibili dati sperimentali relativi alla calibrazione di due barre di controllo del reattore.

Neutronica e Codici Monte Carlo

La grandezza caratteristica sfruttata per l'analisi di un reattore è la *reattività*, definita a partire dal coefficiente di moltiplicazione, il quale rappresenta il rapporto fra il numero di fissioni per una generazione neutronica e quello relativo alla generazione precedente. In base al valore di reattività si possono definire diverse condizioni in cui viene operato il reattore: rispettivamente, *criticità* per valori nulli di reattività, *supercriticità* per valori positivi ed inferiori all'unità e *sottocriticità* per valori negativi. Per quanto riguarda la determinazione della reattività inserita tramite, per esempio, la movimentazione delle barre all'interno del reattore, è possibile trarre il valore della reattività inserita tramite il *metodo del periodo*, il quale è stato sfruttato anche in sede sperimentale per quanto riguarda i dati sfruttati per la validazione del modello sviluppato nell'ambito di questo lavoro di tesi. Questo metodo si basa sull'utilizzo dell'equazione *Inhour*, la pone la reattività in funzione di diversi parametri tra i quali, appunto, il periodo del reattore.

In particolare, il codice utilizzato, Serpent, è un codice Monte Carlo ottimizzato per i calcoli di fisica del reattore e caratterizzato dalla presenza di strutture geometriche pre-implementate disponibili. La più recente versione, utilizzata per sviluppare il modello aggiornato del reattore, presenta inoltre dei vantaggi rispetto alle versioni precedenti in termini di ottimizzazione della memoria e di possibile accoppiamento con codici di termoidraulica e termomeccanica, nonché schemi ottimizzati per i calcoli di burnup.

Il reattore TRIGA Mark II

Il reattore TRIGA (Training Research and Isotope production General Atomics) Mark II è un reattore progettato e prodotto a partire dai primi anni '50 dalla General Atomics

con lo scopo di avere un reattore di ricerca caratterizzato da un'elevata sicurezza intrinseca ed un costo moderato. Il reattore TRIGA Mark II dell'Università di Pavia è stato portato per la prima volta a criticità nel 1965 e viene utilizzato come reattore di ricerca e per la produzione di radioisotopi. Il combustibile è caratterizzato dalla presenza, oltre dell'uranio, di idrogeno e zirconio, che forniscono una capacità moderante che decresce molto rapidamente all'aumentare della temperatura. Il nocciolo è caratterizzato da sei anelli concentrici che ospitano in totale novanta canali che servono per posizionare sia gli elementi di combustibile sia quelli di grafite, sia per inserire la sorgente quando necessario o si prestano al fine di essere utilizzati come canali di irraggiamento. Gli elementi di combustibile originali erano di un unico tipo, denominato 101, mentre ad oggi vi sono tre tipi diversi di barre di combustibile, in particolare 101, 103 e 104, caratterizzate in due casi dalla presenza di dischi di molibdeno e samario, sfruttati come veleni bruciabili. Negli anni passati, sono stati effettuati studi relativi a fenomeni di burnup riguardanti i materiali all'interno del reattore (Chiesa, 2013) e a settembre 2013 vi è stata una riconfigurazione del nocciolo del reattore. Il reattore è caratterizzato dalla presenza di tre barre di controllo, denominate Transient, Shim e Regulating, le quali sono atte rispettivamente alla garanzia della sicurezza del reattore, alla regolazione grezza e alla regolazione fine della reattività. Le variazioni principali fra la configurazione cosiddetta *fresh-fuel* e quella odierna sono legate ai tre tipi diversi di barre presenti oggi, allo svuotamento del canale centrale del reattore, che erano originariamente riempito con acqua, al fatto che i materiali hanno subito fenomeno di burnup e infine alla riconfigurazione avvenuta nel 2013.

Il modello aggiornato

A partire dal modello relativo alla prima versione di Serpent, quindi relativo alla configurazione originale, si è prima verificato che il modello fosse adoperabile anche tramite Serpent 2. Si sono ottenuti risultati compatibili con le criticità sperimentali, osservabili nella figura 1, considerando la presenza di errori statistici e sistematici nell'analisi di quanto ottenuto tramite Serpent.

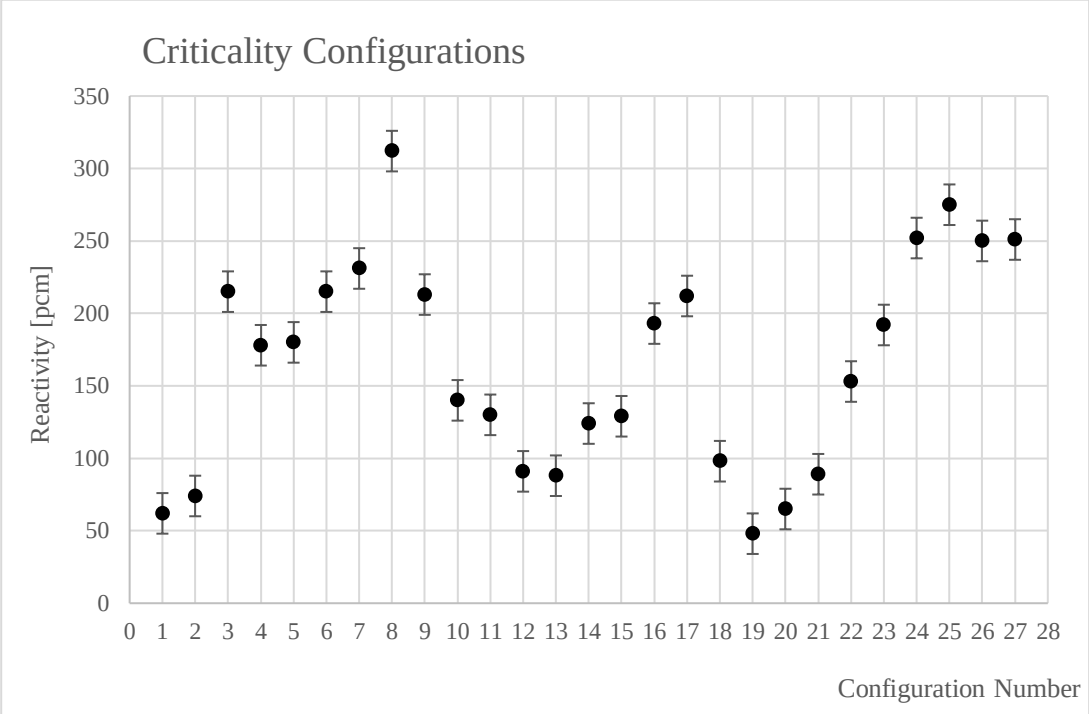

Figura 1: Configurazioni di criticità ottenute tramite Serpent 2 per il modello a combustibile fresco.

La presenza di errori sistematici è legata in primis ai dati, relativi ai materiali, risalenti agli anni '60. Studi effettuati in merito hanno riscontrato un contributo di tali errori, per quanto riguarda le definizioni dei materiali nel modello a combustibile fresco, da quantificarsi come almeno $190\ pcm$ in termini di reattività. Inoltre, va sottolineata l'incertezza che caratterizza i dati, risalenti allo stesso arco temporale citato precedentemente, relativi alle barre di controllo, in particolare alla barra Transient. Considerando i due fattori, cioè le due fonti di incertezza, appena introdotti, i dati relativi alle configurazioni di criticità risultano accettabili, seppur caratterizzati da valori di reattività in alcuni casi elevata.

Si sono successivamente implementate le differenze all'interno del modello, partendo dalle definizioni di nuovi tipi di elementi di combustibile. In secondo luogo sono stati sfruttati i dati ottenuti tramite studi precedenti relativi al burnup aggiornato al 2013 dei materiali presenti nel reattore effettuati tramite MCNP e sono stati adattati in modo da essere utilizzabili tramite Serpent. Anche le variazioni in termini di geometria sono state implementate all'interno del modello. Tramite le figure 2 e 3 è possibile osservare rispettivamente la stessa sezione ottenuta con il modello a combustibile fresco e con il modello aggiornato, ove si possono apprezzare le differenze tra le due

configurazioni per quanto riguarda il nocciolo. Va sottolineato che, nell'intento di poter sfruttare il modello anche per riprodurre condizioni di criticità a piena potenza, sono stati sfruttati studi effettuati in precedenza riguardanti la distribuzione di temperatura all'interno del combustibile discretizzata a seconda dell'anello considerato all'interno del nocciolo e, discretizzando in senso verticale, dividendo gli elementi in cinque sezioni diverse, in modo tale da associare ad ognuno un valore di cross section quanto più fedele alla condizione reale in termini termici. In figura 4 è mostrato un riassunto schematico delle differenze principali fra il modello a combustibile fresco e quello aggiornato alla configurazione del nocciolo del 2013.

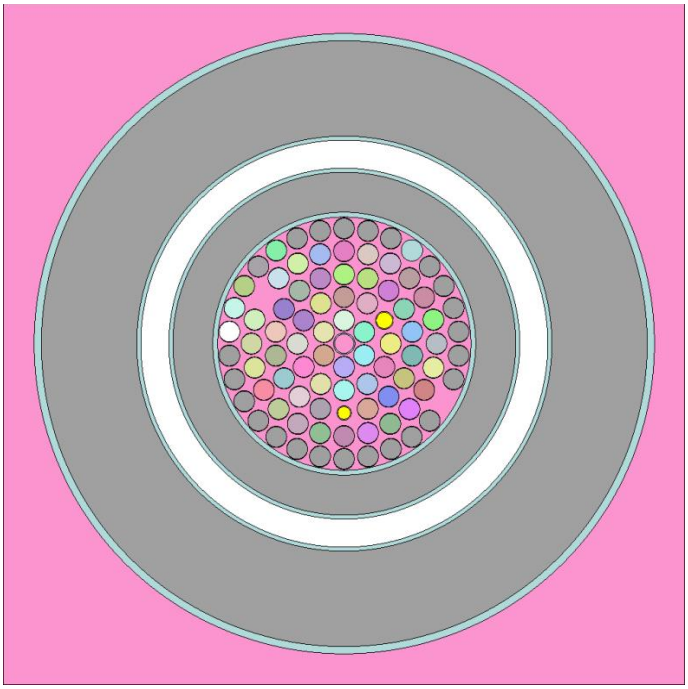

Figura 2: Sezione radiale del reattore TRIGA Mark II ottenuta tramite Serpent 2 per la configurazione originale.

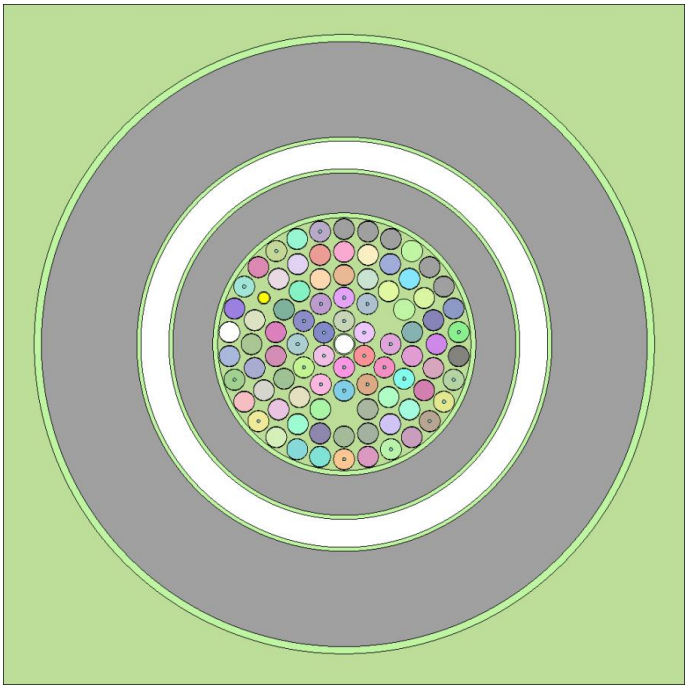

Figura 3: Sezione radiale del reattore TRIGA Mark II ottenuta tramite Serpent 2 per la configurazione aggiornata all'anno 2013.

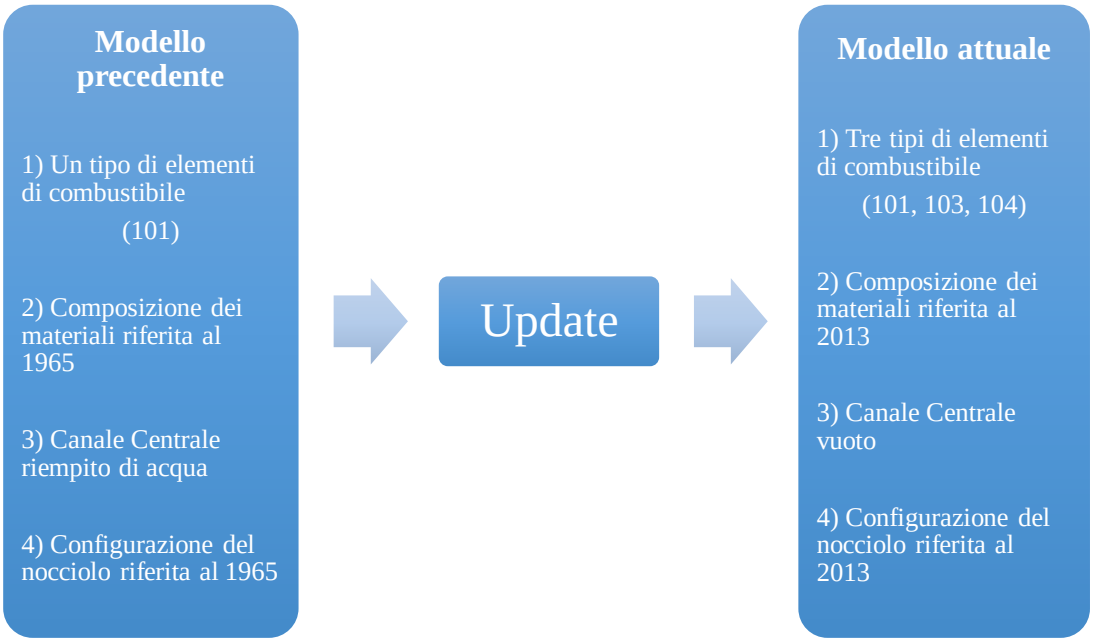

Figura 4: Riassunto schematico della procedura di aggiornamento del modello

Risultati

Per quanto riguarda i risultati ottenuti tramite le simulazioni effettuate sfruttando il modello, è necessario fare menzione delle due fonti principali di incertezza che caratterizzano i risultati. Prima di tutto, l'errore statistico associato alle simulazioni Monte Carlo stesse, il quale è proporzionale all'inverso della radice del numero di vite neutroniche simulate. In secondo luogo, vi è l'influenza di errori di tipo *sistematico* legati alle incertezze riguardanti i dati relativi alle composizioni e alle densità dei materiali costituenti il reattore e sfruttati per sviluppare il modello. Questo tipo di errore è stato quantificato in termini di reattività come circa $190\ pcm$ per quanto riguarda la condizione a combustibile fresco, seppur si tratti di un limite inferiore nel senso stretto di errore sistematico per il lavoro in analisi. Infatti, i dati relativi ai materiali sfruttati nel modello relativo a questo lavoro di tesi e alle densità degli stessi sono stati in precedenza sottoposti a calcoli di burnup tramite codici Monte Carlo. A seguito di ciò, per ottenere una quantificazione fedele degli errori sistematici relativi ai materiali, bisognerebbe tenere in considerazione la propagazione dell'errore dovuta ai suddetti calcoli.

I primi dati riprodotti tramite simulazione sfruttando il modello sviluppato sono stati relativi alla prima configurazione di criticità a piena potenza e al core excess, per i quali si è effettuato un confronto sia con i dati sperimentali sia con risultati ottenuti tramite altri studi effettuati con MCNP (Chiesa, 2013). Per quanto riguarda la riproduzione della configurazione di criticità, il risultato ottenuto $1{,}99996\ pcm \pm 7\ pcm$, dove si è tenuto in considerazione l'errore statistico del Monte Carlo si è mostrato in accordo con i dati sperimentali; ciò è stato riscontrato anche per il risultato pertinente al core excess, considerando un intervallo di 1σ attorno al risultato ottenuto tramite Serpent.

Per quanto riguarda l'incertezza relativa ai risultati ottenuti tramite simulazione con Serpent, essa dipende dal numero di cicli che vengono effettuati dal software ed il numero di neutroni generati dalla simulazione per ogni ciclo. Vi è una relazione di proporzionalità inversa, infatti, fra la suddetta incertezza e la radice del prodotto di queste due ultime grandezze. Per ogni simulazione effettuata nell'ambito di questo lavoro di tesi, sono stati generati 8000 cicli da 40000 neutroni l'uno. L'incertezza riguardante gli output forniti da Serpent si è quindi attestatata sempre attorno a $7\ pcm$.

Risultati per la Criticità

In seguito alla riproduzione della prima criticità a piena potenza e del core excess, sfruttando dei dati sperimentali relativi rispettivamente agli anni 2015 e 2018, si è cercato di riprodurre, tramite l'utilizzo del modello aggiornato, alcune configurazioni di criticità. Le configurazioni sono state ottenute in sede sperimentale in occasione della calibrazione di due barre di controllo, i cui risultati sono discussi in seguito. In figura 5 sono mostrati i dati relativi a quanto ottenuto tramite Serpent.

Dalla figura, si può osservare come le configurazioni relative ai dati dell'anno 2018 presentino un offset verso valori di reattività superiori, questo dovuto probabilmente al fatto che i materiali all'interno del reattore hanno subito fenomeni di burnup di cui il modello non tiene conto, essendo riferito all'anno 2013. Va sottolineato, tuttavia, che nei limiti dell'incertezza statistica e sistematica entrambi i set di dati risultano in accordo con quanto ottenuto a livello di criticità sperimentale.

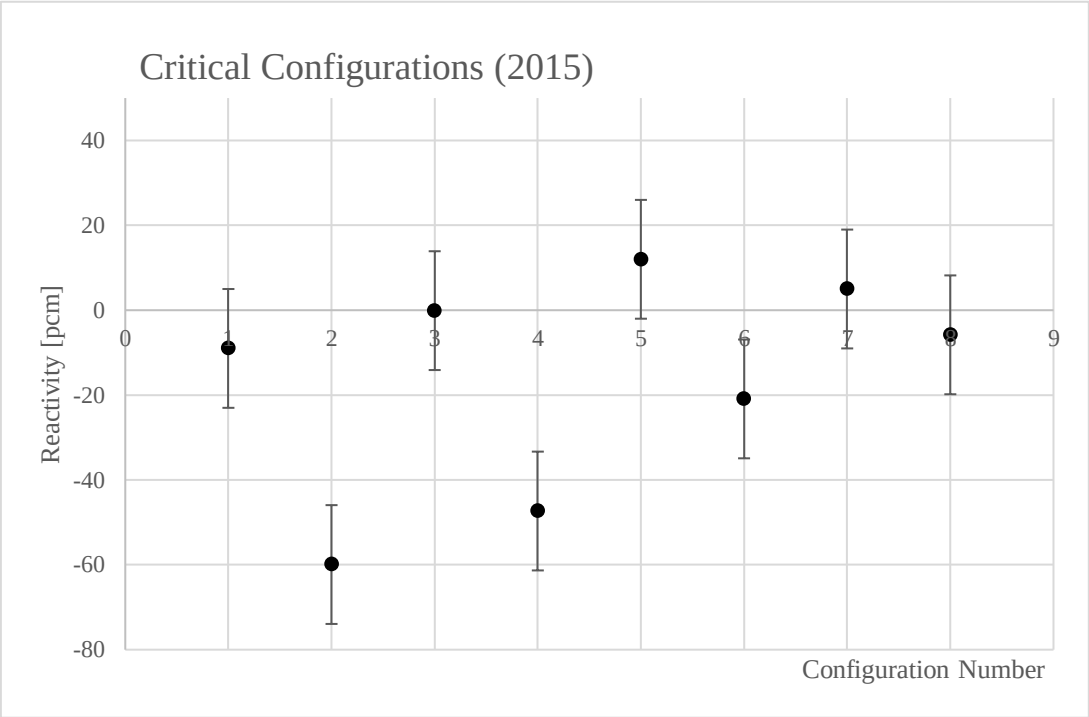

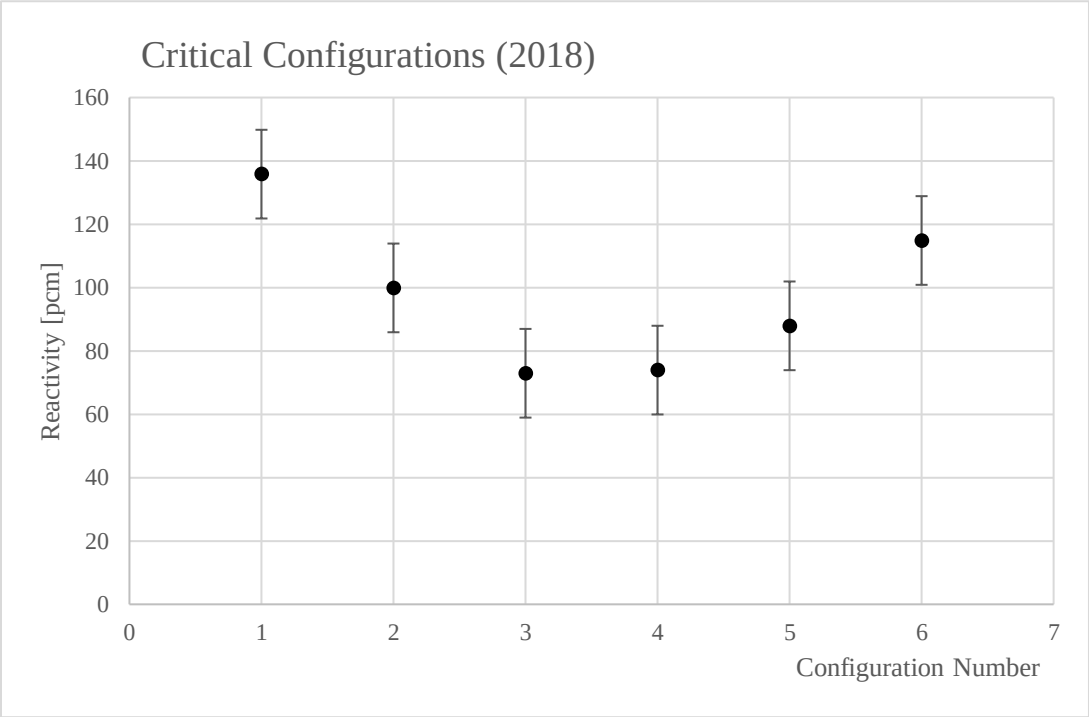

Figura 5: Risultati per la riproduzione delle configurazioni di criticità relative rispettivamente agli anni 2015 e 2018.

Risultati per la Calibrazione

Un'ulteriore validazione del modello si è ricercata tramite il confronto con dati relativi alla calibrazione della barra di controllo Regulating e della parziale calibrazione della barra di controllo Shim, effettuate sperimentalmente negli anni 2015 e 2018 tramite metodo del periodo. A livello prettamente procedurale, la calibrazione viene effettuata partendo da una condizione di criticità con la barra Transient completamente estratta, la barra Shim parzialmente inserita e la barra Regulating totalmente inserita. Vengono poi progressivamente effettuate inserzioni di reattività estraendo parzialmente la regulating e misurando il tempo necessario per ottenere una determinata crescita di potenza. Il dato misurato verrà conseguentemente manipolato, in modo tale da ottenere la reattività inserita tramite movimentazione della barra Regulating. Successivamente, la barra Shim viene proporzionalmente posta in maggiore profondità nel nocciolo in modo tale da ristabilire una condizione di criticità. Le precedenti operazioni vengono ripetute fino a completa estrazione della barra Regulating. È possibile quindi ottenere, a partire dai dati misurati, curve di calibrazione sia integrale che differenziali per la barra Regulating. Per quanto riguarda la barra Shim, è possibile effettuare una calibrazione solo parziale, non effettuando una corsa completa della barra di controllo. Per quanto riguarda gli errori legati alle procedure sperimentali, si è tenuto conto dell'incertezza legata a tutti a parametri necessari ad ottenere la reattività a partire dalle misure sperimentali. Sfruttando la tecnica proposta da Moffat, che prevede che l'incertezza di un parametro ottenuto tramite combinazione di più grandezze si calcoli tenendo in considerazione i limiti superiori e inferiori di tutti i parametri coinvolti e affetti da incertezza, si è calcolato l'errore per ogni punto sperimentale di calibrazione in termini di reattività.

Le condizioni di criticità per i due set di dati sperimentali relativi agli anni 2015 e 2018 sono stati riprodotti, ottenendo risultati in entrambi i casi in accordo con i dati sperimentali considerando sia l'errore statistico Monte Carlo sia l'incertezza legata agli errori sistematici. Si sono poi riprodotte le curve di calibrazione integrale, effettuando per quanto possibile una ricostruzione per quanto riguarda la barra Shim, avendo a disposizione solo dati differenziali e quindi parziali. I dati relativi alla calibrazione per quanto riguarda la barra Regulating sono apprezzabili in figura 6 e 7.

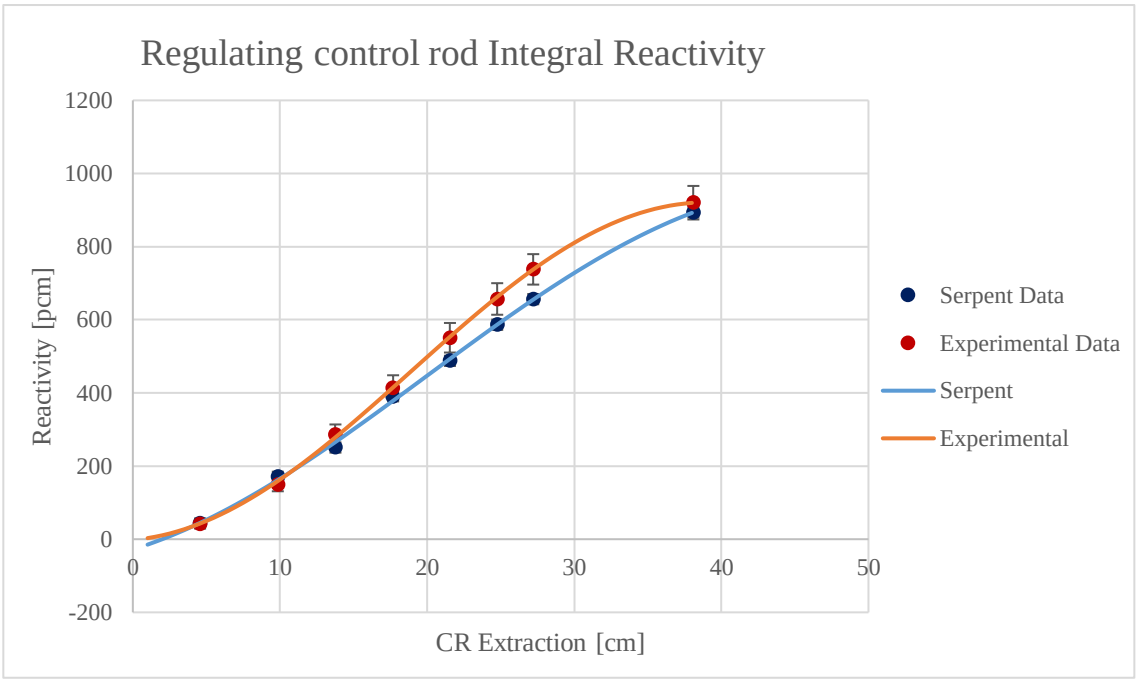

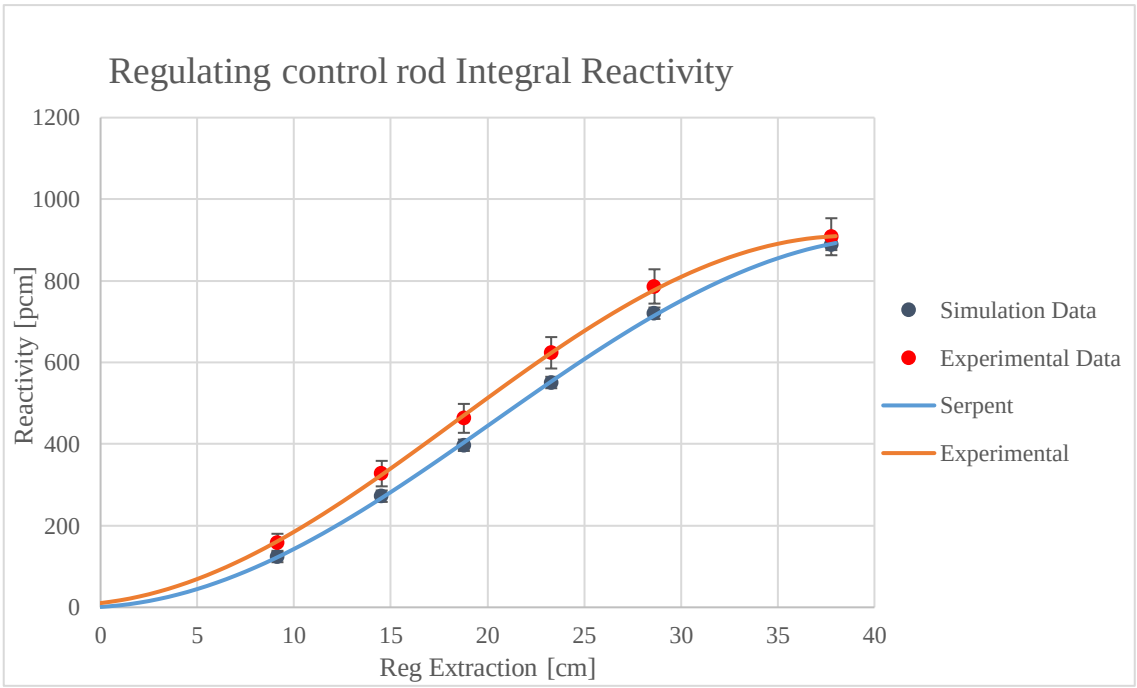

Figura 6: Curve di calibrazione Integrale per la barra Regulating ottenute sperimentalmente e tramite Serpent con il modello sviluppato rispettivamente per i dati relativi all'anno 2015 e 2018.

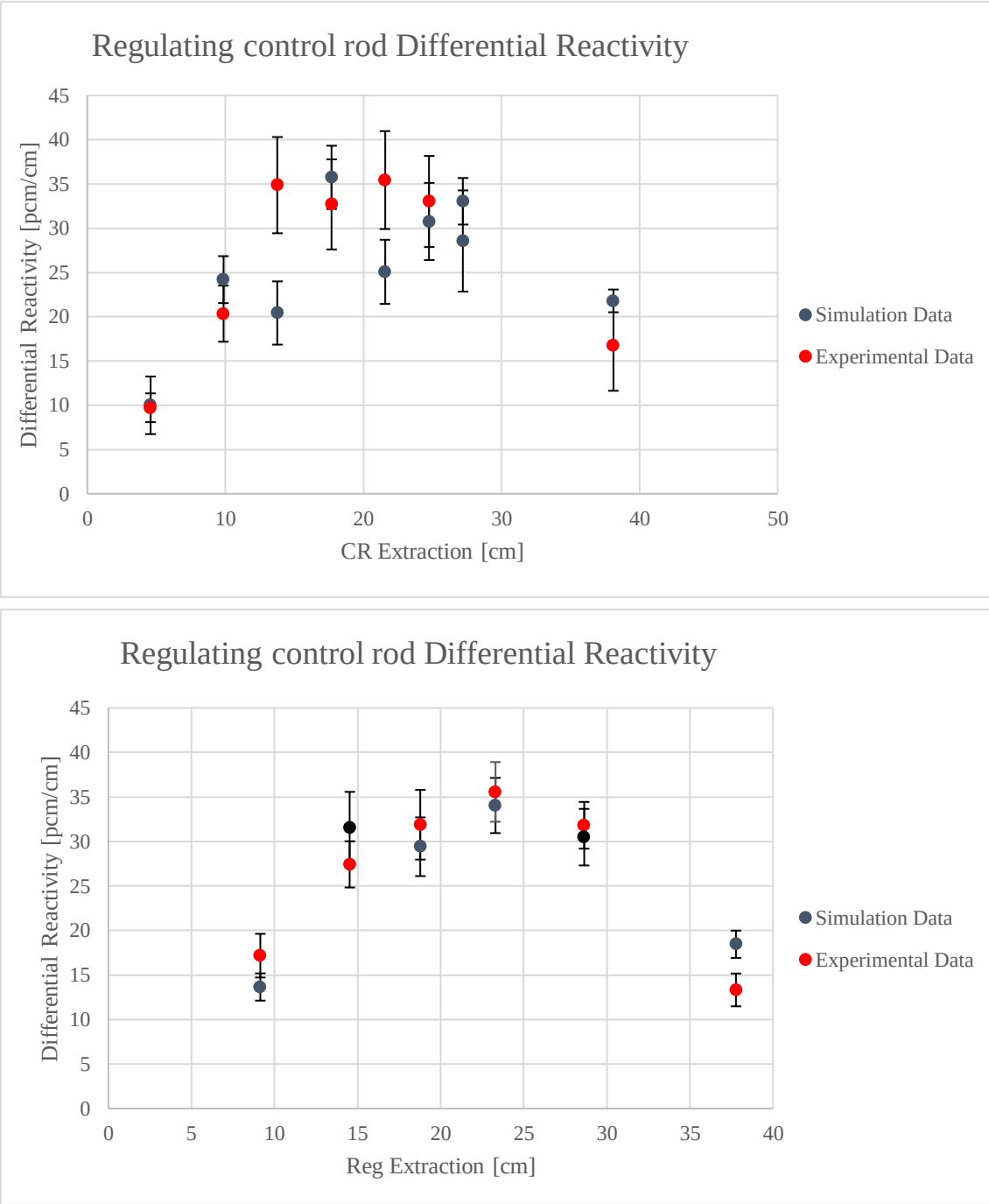

Figura 7: Dati relativi alla reattività differenziale per la barra Regulating ottenuti sperimentalmente e tramite Serpent con il modello sviluppato rispettivamente per i dati relativi all'anno 2015 e 2018

I dati ottenuti tramite simulazioni a partire dal modello sviluppato si sono rivelati in buon accordo con i dati sperimentali per entrambi i set, cioè sia per il 2015 che per il 2018.

Nonostante sia giusto sottolineare la presenza dell'offset rispetto alle configurazioni di criticità introdotto precedentemente, è altrettanto fondamentale ricordare che, tenendo conto delle fonti di incertezza prese in analisi per questo lavoro, il modello risulta valido nella riproduzione dei dati relativi alla reattività integrale e differenziale. Nel caso si consideri, poi, la presenza di errori sistematici, i quali forniscono un contributo che si attesta almeno a $190\,pcm$, tutte le configurazioni di criticità risultano in accordo con i dati ottenuti sperimentalmente in un intervallo 1σ.

Considerando la seconda barra di controllo, in figura 10 e 11 è possibile osservare i dati ottenuti per quanto riguarda la barra Shim sia sperimentalmente che tramite Serpent. Tramite i dati differenziali è possibile osservare come, in particolare per l'anno 2018, il modello sia in accordo con i dati sperimentali. Si è inoltre effettuato un test χ^2 per valutare la bontà degli output, in termini di reattività differenziale, provenienti dal modello rispetto a quelli sperimentali e i risultati sono stati soddisfacenti, soprattutto per i dati relativi all'anno 2018. In tabella 8 e 9 sono visibili i risultati ottenuti relativi al test χ^2, a seguito del quale, prendendo come valore di riferimento per il p-value il 5%, solo il dato relativo alla calibrazione della barra Shim effettuata nel 2015 ha ottenuto un risultato inferiore. Considerando i risultati nell'insieme, tuttavia, si può confermare che quanto ottenuto tramite Serpent è in buon accordo con i dati sperimentali.

Barra di controllo	$\boldsymbol{\chi^2}$	$\boldsymbol{\nu}$	**p-value**
Regulating	13,16	8	10%
Shim	17,03	7	1,9%

Tabella 8: Risultati del test χ^2 relativo a dati sperimentali e simulati per l'anno 2015.

Barra di controllo	$\boldsymbol{\chi^2}$	$\boldsymbol{\nu}$	**p-value**
Regulating	7,21	6	30%
Shim	5,35	5	40%

Tabella 9: Risultati del test χ^2 relativo a dati sperimentali e simulati per l'anno 2018.

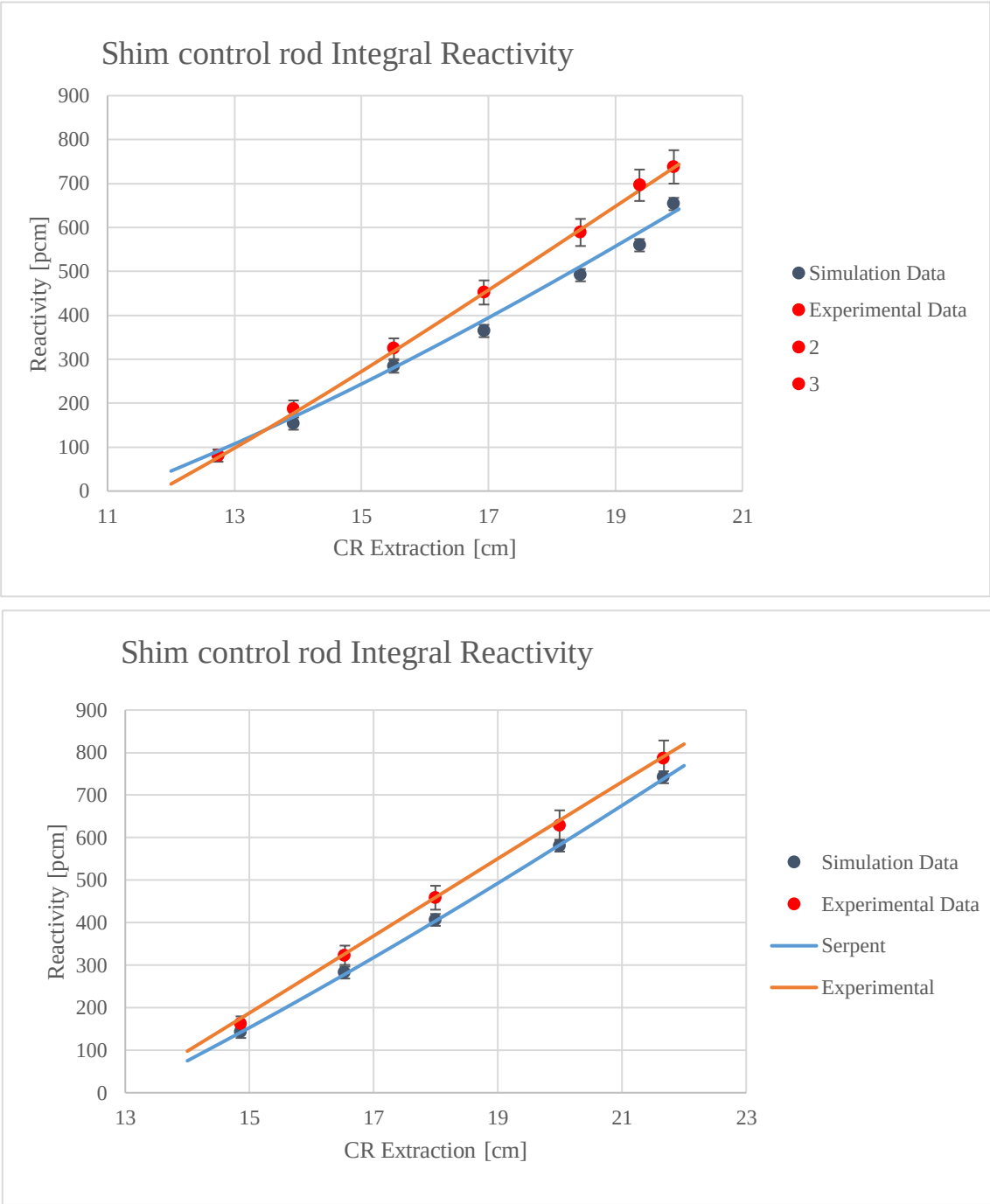

Figura 10: Curve di calibrazione Integrale parziale per la barra Shim ottenute sperimentalmente e tramite Serpent con il modello sviluppato rispettivamente per i dati relativi all'anno 2015 e 2018.

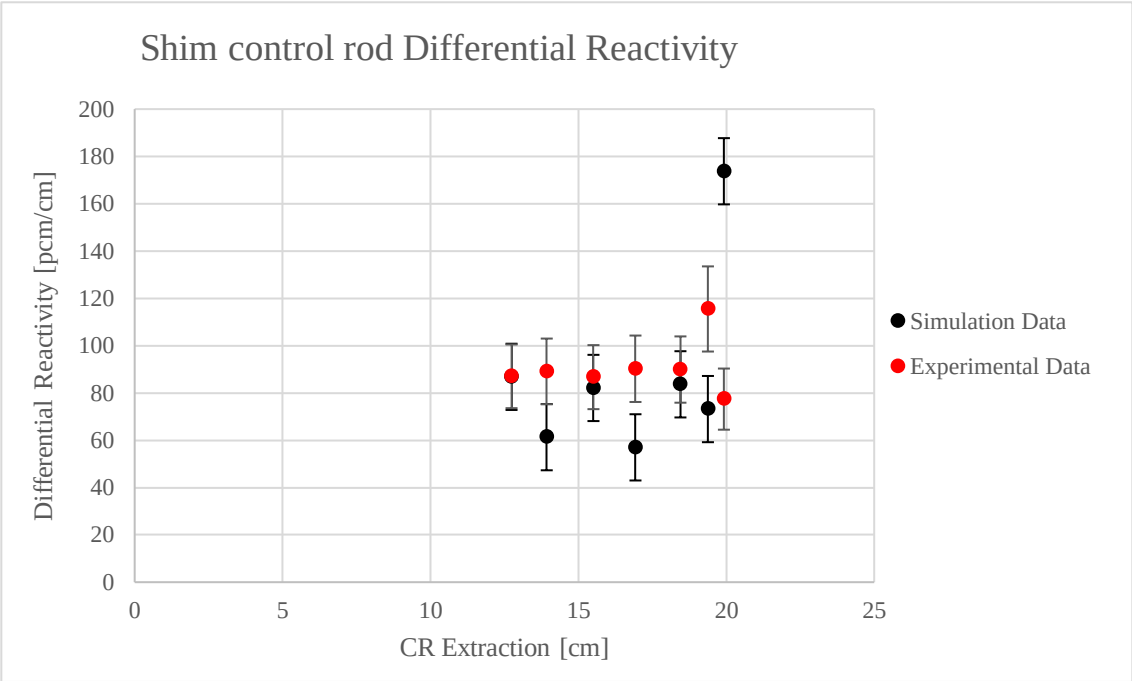

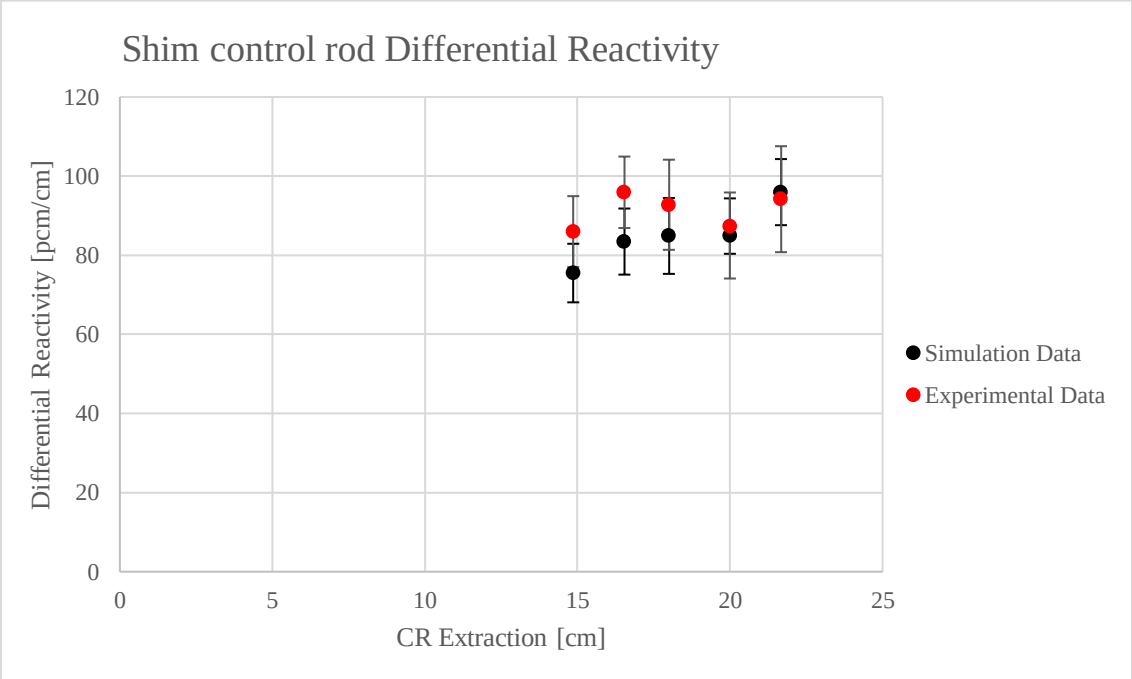

Figura 11: Dati di calibrazione differenziale per la barra Regulating ottenute sperimentalmente e tramite Serpent con il modello sviluppato rispettivamente per i dati relativi all'anno 2015 e 2018.

Dal punto di vista della calibrazione delle barre di controllo, il modello sviluppato si è dimostrato quindi un valido strumento nel simulare le variazioni di reattività introdotte tramite le barre di controllo analizzate.
In generale, considerando non solo i risultati ottenuti non solo per la calibrazione, ma anche per le configurazioni di criticità sia a piena potenza che a bassa potenza e il core excess, il modello aggiornato è risultato valido e in accordo con i dati sperimentali.

Conclusione

Il lavoro di tesi qui riassunto ha avuto lo scopo di sviluppare un modello aggiornato all'ultima configurazione del nocciolo per il reattore TRIGA Mark II dell'Università di Pavia. Grazie a lavori già sviluppati in precedenza riguardanti la configurazione del reattore a combustibile fresco e a studi effettuati sui materiali presenti all'interno del reattore, è stato possibile sviluppare in modello in maniera aderente all'attuale composizione dei materiali e configurazione del nocciolo. Tramite confronti code-to-code con lavori svolti con MCNP e comparazione dei risultati ottenuti con dati sperimentali è stato possibile validare il modello entro gli intervalli di incertezza che tenessero conto sia di errori di tipo sistematico sia di tipo statistico. Gli output relativi alle configurazioni riprodotte sono risultati in buon accordo con i dati sperimentali, seppur osservando un leggero offset rispetto alla criticità nella riproduzione di configurazioni relative al 2018. Riferendosi il modello a dati per i materiali relativi al 2013, è possibile ipotizzare che i materiali stessi abbiamo subìto effetti di burnup. Nonostante ciò, quanto ottenuto dalle simulazioni di criticità e da quelle relative alle calibrazioni delle barre di controllo è in accordo con i dati sperimentali, mostrando come il modello aggiornato del reattore TRIGA Mark II possa essere utilizzato come strumento di analisi dell'attuale configurazione del reattore. Futuri sviluppi e applicazioni di questo modello coinvolgono il suo utilizzo per calcoli di burnup e accoppiamento dello stesso con la termoidraulica, con l'obiettivo di ottenere una descrizione completa del sistema.

Contents

Introduction

During the last decades, the approach to physics and to solving physics-related problems has been relying on simulation codes, thanks to their ability to involve different and various scenarios concerning all types of phenomena, which can often be a time-consuming task for pure analytical methods. In the field of neutronics simulation codes, the first distinction that can be introduced lays between deterministic codes and Monte Carlo codes. The formers solve the transport equations exploiting some approximations, while the latter simulate the entire neutron life, for each neutron in the system. The feature that makes Monte Carlo codes more advantageous compared to deterministic codes lays in the accuracy and flexibility. Since no rough approximation is exploited, uncertainty is strongly reduced when adopting Monte Carlo codes over deterministic ones. For Monte Carlo codes, in fact, the transport equation in implicitly solved when performing the simulation. Another factor that plays a significant role in choosing the most suitable code for neutronics simulation purposes is the computational burden related to Monte Carlo codes. In fact, the memory requirements and computational expense related to the simulations characterizing Monte Carlo codes are rather high. However, with the recent development and increasing availability of more sophisticated and computationally-powerful computers, overcoming the computational burdens previously cited is now more feasible. The higher degree of accuracy and superior flexibility, along with a nowadays more approachable use, have made Monte Carlo codes the predominant choice in many areas. For what concerns models themselves, the need for verification and validation is a fundamental subject when considering their application on actual reactors. Research reactors have a crucial role when developing such models, because they provide a reliable, though practical, validation instrument.

The TRIGA Mark II reactor of the University of Pavia was already exploited to this purpose for a model pertaining the fresh-fuel configuration of the reactor, developed with the Monte Carlo code Serpent

The aim of the present thesis work is to develop a new model for the TRIGA Mark II reactor, updated to last configuration. The calibration pertaining one of the control rods and the partial calibration of another control rod exploiting the model have been part of the focuses of this work as well, in order to perform a benchmark analysis with experimental results pertaining rods calibrations and other parameters such as the core excess. The just cited experimental results are to be employed as verification and validation tools for the model.

In the first chapter, the basic concepts behind neutronics, and on which Monte Carlo codes for the purpose of this work are based, are explained. In the second chapter, Monte Carlo codes are presented and an exploration of their main features together with the description of Serpent code is performed. In the third chapter, the characterization of the TRIGA reactor this work has been developed for is present, alongside with an explanation on how the model describing this reactor has been developed. In the fourth and last chapter, results concerning Monte Carlo simulation for different cases are shown. Data obtained through MCNP are available for a code-to-code comparison and experimental benchmarks analysis results are presented as well. Technical procedures regarding the experimental datasets collection are also rendered in the fourth chapter. Final considerations are left to the conclusions.

Chapter 1

Theoretical background of neutronics

Nuclear reactor are complex systems and their complete analysis requires a thorough knowledge of different subjects such as neutronics, thermal-hydraulics and thermo-mechanics. Understanding the phenomena within a nuclear reactor core is directly related to the understanding of neutronics, whose basic aspects will be explained in this chapter, in order to cover the concepts Monte Carlo codes exploited for this thesis work are based on.

Neutron Interaction with matter

In dealing with phenomena regarding neutron behavior within a reactor, the proper way of analyzing all its features should be by means of the so called *transport equation*, whose detailed description is out of the scope of this introduction. It will be further specified in the next chapters that the simulations performed for this thesis work exploit and have as a basis the involvement of all possible interactions neutrons can undergo along their path. A proper, even though quite superficial, understanding of how such interactions take place seems adequate in order to have a closer insight on the principles the previously mentioned simulations are based on.

There are three main types of interactions (Lamarsh, 1966) that can be identified between neutrons and matter:

- *Absorption*: this kind of interaction is a general term referring to all those reactions in which no neutron is observed afterwards. There can be different examples, such as radiative capture (n,γ), (n,p), (n,α), or fission, which concerns the absorption of a neutron by a heavy nucleus with the subsequent emission of fragment-nuclei, free neutrons, a given amount of energy release and other reaction products.
- *Elastic Scattering (n,n)*, where the target nucleus remains in the same condition after the interaction both in the isotopic composition and from an energetic point of view.
- *Inelastic Scattering (n,n')*, in which kinetic energy does not obey a conservation principle and the target nucleus results in an excited state after the interaction.

In order to properly consider all the reactions that can take place involving neutrons and a certain material in a probabilistic frame, the definition of *cross section* becomes useful. Let us consider a target defined by an area S and a thickness x, with n as the atomic volumetric density, on which there is an incident neutron beam of intensity I. The reaction rate within the material, can be defined as:

$$R = \sigma n I S x \quad \left[\frac{reactions}{s}\right]$$

It is immediately observable that the rate is proportional to physical quantities listed above through a proportionality constant σ, which is in fact an area whose dimensions are usually expressed in *barns* ($1b = 10^{-24} cm^2$). It can also be underlined that the intensity of the neutron beam as a function of the target thickness follows the exponential trend hereafter:

$$I(x) = I_0 e^{-N\sigma x}$$

where I_0 is the incident beam intensity.

The product $N\sigma$ stands for the interaction probability per unit path and it can also be called *Macroscopic Cross Section* Σ. Starting from this relation and inverting it, the neutron *Mean Free Path* λ can be obtained:

$$\lambda = \frac{1}{\Sigma} = \frac{1}{N\sigma} \quad [cm]$$

Cross sections can be defined individually for each process and then summed to obtain the total cross section for all the phenomena concerning the interaction between two elements:

$$\sigma_t = \sum_i \sigma_i$$

Fission Reactions

As previously mentioned, nuclear fission is the process where a heavy nucleus separates into two or more lighter nuclei releasing energy, gamma rays and free neutrons.

When reasoning in terms of binding energy as a function of mass number, it can be observed that this quantity decreases for A greater than 50, which means that when a heavy nucleus splits into lighter ones, there is a considerable energy gain, because of their higher binding energy.

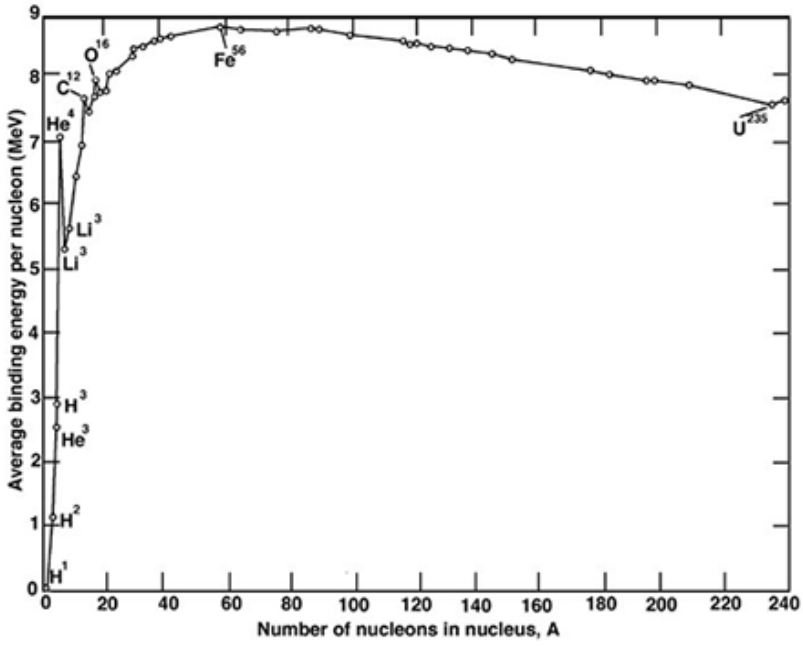

Figure 1.1: Average binding energy per nucleon versus atomic mass number.

Despite its energy advantages, spontaneous fission is sporadically observed and the way most fissions occur is following a triggering event that brings the system above a certain threshold also known as *critical energy* E_c. This value basically represents the energy barrier that must be overcome to obtain fission.

The configuration obtained after the absorption of a neutron by an heavy nucleus has a total energy which is computable as the sum of the original nucleus binding energy and the neutron energy. If the former is higher than the critical energy, there are no restraints for what concerns neutron energy and the nucleus is called *fissile*. On the other hand, nuclei with binding energy below fission critical energy are defined as *fissionable* and neutrons are subject to certain energy requirements. Examples of fissile isotopes are ^{235}U, ^{233}U, ^{239}Pu, while nuclides such as ^{238}U and ^{232}Th are fissionable.

As already stated, right after fission, alongside fission fragments there is the production of gamma rays and a given number of neutrons which are called *prompt*, whose energy spectrum has an average value of about 2 MeV.

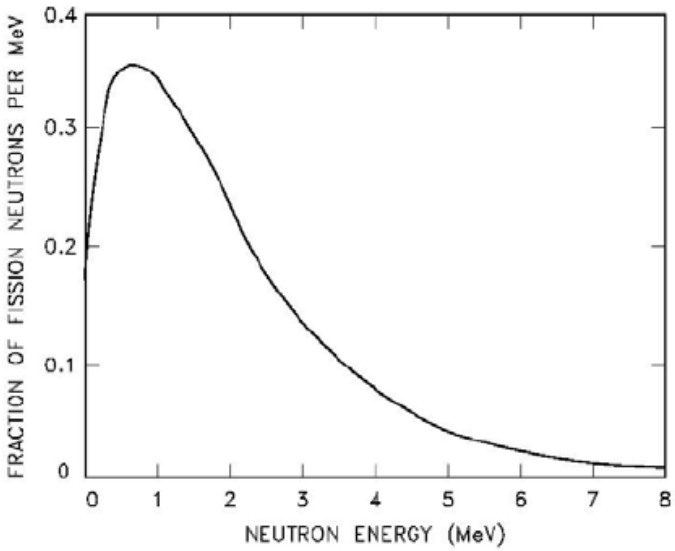

Figure 1.2: Fission neutrons energy spectrum.

Since fission fragments are featured by a strong excess in neutron content, after a certain amount of time the emission of the so called *delayed* neutrons is observed through β^- decay, which introduces also electrons and neutrinos as secondary fission products.

Almost all energy (80%) released in fission processes is carried by fission products as kinetic energy, which can be therefore collected as thermally. The 20% energy left is split pretty equally among other products. It is safe to say that the fraction of recoverable energy for this process is close to 1, which makes it favorable in terms of power production.

Form	**Emitted Energy** [MeV]	**Recoverable Energy** [MeV]
Fission Products	168	168
Electrons	8	8
γ-Rays	14	14
Neutrinos	12	-
Fission Neutrons	5	5
Capture γ-Rays	-	3-12
Total	**207**	**198-207**

Table 1.3: Emitted and Recoverable energy, expressed in MeV, for ^{235}U fission.

Thermal Motion and Chemical Binding effects

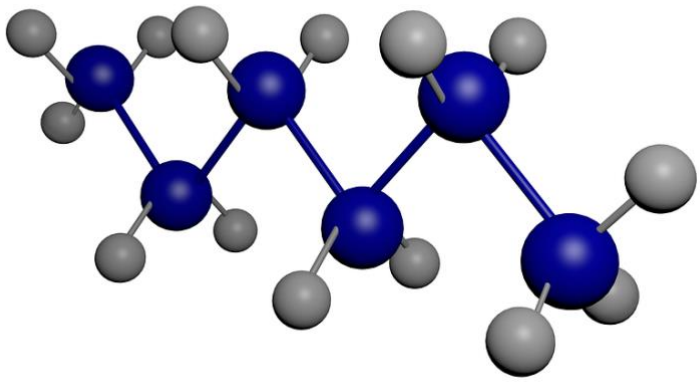

When treating cross sections and in general when modeling neutron-matter interactions, there are two peculiar features to be taken into consideration:

A. *Thermal Motion of Target Nuclei*

Let us consider a material for which the absorption cross section is negligible compared to the scattering one and let us focus on elastic scattering phenomena only, following which there will be, at a certain point, a thermal equilibrium condition. In this particular condition, there is a continuous energy transfer (a sort of back-and-forth transfer) between neutrons and target nuclei, whose thermal energy is proportional to temperature through the Boltzmann constant k.

Treating this case with a free-gas model describing atoms within matter, a direct proportionality relation between interaction cross sections and temperature can be found and the *average cross section* can be expressed as:

$$\overline{\sigma} \propto \frac{\sqrt{T}}{v}$$

where T is the material temperature and v is the neutron velocity when impacting on the material.

B. *Chemical Binding Effects*

It is experimentally observed that at very low energies, usually in the order of the eV, cross sections values result higher for bound nuclei than for free ones.

When considering two particles that are bound together, it can be shown that the cross section behavior has the following trend:

$$\sigma_{bound} = \left(\frac{A+1}{A}\right)^2 \sigma_{free}$$

This phenomenon will therefore be critical for light nuclei, most of all for hydrogen.

Another effect worth mentioning is related to solid lattice structures that can be found in graphite, beryllium and uranium oxide and that provide an effect called *Bragg Scattering*. When considering a neutron impacting on a molecule or on a general bound structure, the possibility of exciting vibrational or rotational modes of the target must be taken into account. Since there is no conservation of kinetic energy, this effect falls in the category of inelastic scattering, for which a cross section $S(\alpha, \beta)$ can be defined. The terms α and β refer respectively to *momentum transfer* and *energy transfer* and they both depend on temperature. There is therefore the need of defining these cross sections at different temperature when modeling these processes.

The understanding and proper physical quantification of these effects are fundamental when modeling materials in order to simulate accurately reactor behavior, most of all when describing operation at full power.

Neutron Balance and Reactivity

In order for power production to be constant, a stability condition must be reached, for which exactly one neutron is produced at each fission and it subsequently induces another fission event.

A *multiplication factor* k can be defined, which is computed through the ratio of the number of fissions in one neutron generation to the number of fissions in the preceding one. This factor can take all possible non-negative values and its domain can be subdivided into three regions that identify three different operating conditions:

- $k \in [0, 1)$ The system is defined as *subcritical*: at each generation the number of fissions decreases.
- $k = 1$ The system is called *critical*: the number of fissions is constant in time.
- $k \in (1, +\infty)$ The system is said to be *supercritical*: the reaction diverges as the number of fissions increase at each generation.

Starting from the multiplication factor, another quantity of interest can be introduced; *reactivity* can be defined as:

$$\rho = \frac{k - 1}{k}$$

As it can be drawn from the previous expression, reactivity values span from minus infinity to one and *criticality condition* is reached when $\rho = 0$.

In order to obtain and maintain a properly stable reaction, an equilibrium between neutrons produced through fission and those that are lost by leakage and absorption must be achieved. The field that most focuses on the measurement of the system's reactivity is called *reactor dynamics* and it analyzes all those factors that affect this quantity.

A very important role in controlling reactivity is played by *delayed neutrons*, which appear approximately in six group which can be discretized in terms of energy, half-life[1] and fraction (β_i) with respect to the total number of emitted neutrons.

[1] Half-lives and decay constants actually refer to delayed neutrons precursors, see next footnote.

Group	Half-Life [s]	Decay Constant λ_i [s^{-1}]	Energy [keV]	Yield Neutrons per Fission	Fraction (β_i)
1	55.72	0.0124	250	0.00052	0.000125
2	22.72	0.0305	560	0.00342	0.001424
3	6.22	0.111	405	0.00310	0.001274
4	2.30	0.301	450	0.00624	0.002568
5	0.610	1.14	-	0.00182	0.000748
6	0.230	3.01	-	0.00066	0.000273
Total				0.0158	0.0065

Table 1.4: Delayed neutron data for thermal fission in ^{235}U.

It needs to be noted that the values that can be found in table 1.4 are not constant universally whatsoever but, being them a function of fuel features, they change depending on the reactor that is being analyzed. For the TRIGA Mark II of the University of Pavia, the total β value equals $730\ pcm \pm 35\ pcm$. Reactivity is usually expressed in pcm[2], but it can also be expressed in relation to the delayed neutron total fraction β using a measuring unit known as *dollars*:

$$\rho\ [\$] = \frac{\rho\ [pcm]}{\beta\ [pcm]}$$

This type of measuring unit becomes useful when considering *prompt criticality*, which is in fact a condition where the reactor is critical without any contribution needed from delayed neutrons and it is reached when $\rho = \beta$, therefore when $\rho = 1\$$. In general, considering an infinite and homogeneous reactor, the power produced at time t via nuclear fission is directly proportional to neutron concentration at time t, $n(t)$. Both neutron concentration $n(t)$ and *precursor*[3] concentration[4] $C_i(t)$ must obey these constraints:

[2] $1\ pcm \triangleq 0.00001$.
[3] Precursors are defined as those fission-product nuclei that decay and consequently emit delayed neutrons.
[4] Concentrations are expressed in $[cm^{-3}]$.

$$\begin{cases} \dfrac{dn(t)}{dt} = \dfrac{k_\infty(1-\beta)-1}{l} n(t) + \displaystyle\sum_{i=1}^{6} \lambda_i C_i(t) \\ \dfrac{dC_i(t)}{dt} = \dfrac{k\beta_i}{l} n(t) - \lambda_i C_i(t) \end{cases}$$

Where k_∞ is the multiplication factor for an infinite reactor, hence with no leakages involved, l is the prompt neutron lifetime, while β_i and λ_i are respectively the neutron fraction and decay constant for the delayed neutrons' i^{th} group.

Considering all the delayed neutrons groups, there are in total seven equations to be solved and the solutions to be looked for are of the following type:

$$\begin{cases} n(t) = Ae^{\omega t} \\ C_i(t) = C_i e^{\omega t} \end{cases}$$

A general solution can be obtained as the linear combination of all the possible ones. Working these expressions into the original equations and searching for a solution in terms of reactivity, the *Inhour Equation*[5] (Duderstadt and Hamilton) can be found:

$$\rho_\infty = \frac{\omega l}{1+\omega l} + \frac{\omega}{1+\omega l} \sum_{i=1}^{6} \frac{\beta_i}{\omega + \lambda_i}$$ [6]

Having set seven equations to start with, there will be seven solutions for ω.

A good instrument in order to understand how these physical phenomena work is plotting ρ versus ω and comparing the resulting neutron population trends for different reactivity values. An example of such a plot is shown in figure 1.5.

[5] The eigenvalues ω were traditionally expressed in $[h^{-1}]$ and from this inverse-hour measuring unit eventually the name *Inhour* was born.

[6] $\rho_\infty = \frac{k_\infty - 1}{k_\infty}$ is defined as the reactivity for an infinite reactor.

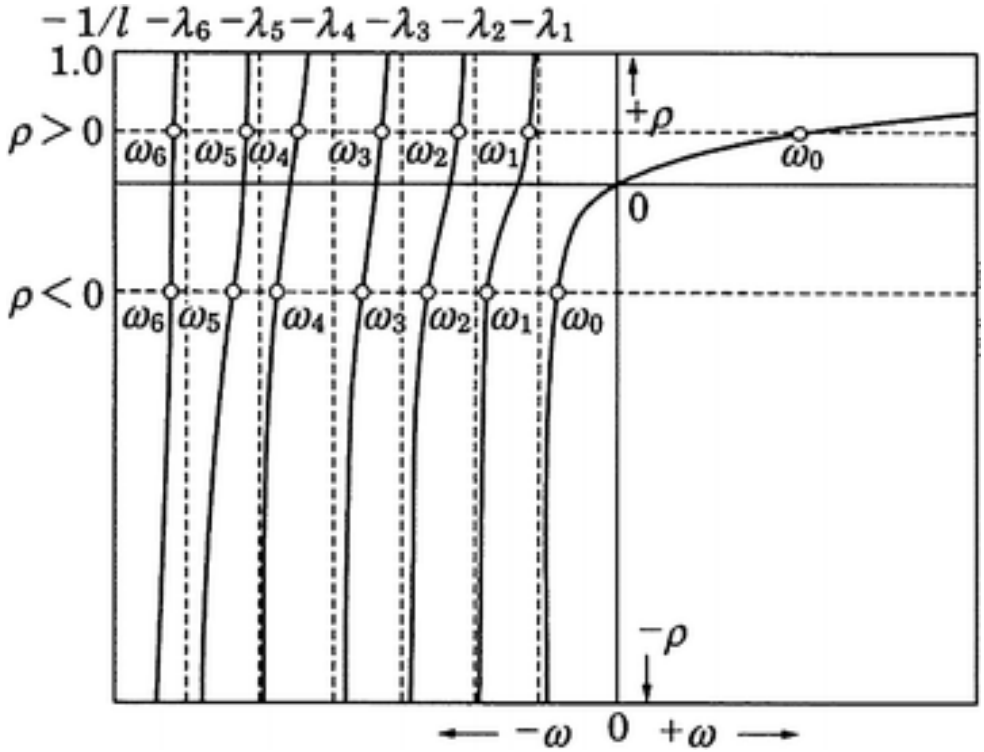

Figure 1.5: Inhour Equation solutions expressed in terms of reactivity versus ω.

In case of negative reactivity values, all solutions are negative, while when ρ is greater than zero, the results are the same except for ω_1, which is positive.

The general thermal power trend can be written as:

$$P(t) = P(0)\sum_{i=1}^{7} A_j e^{\omega_j t}$$ [7]

A common case that serves well as an example is one with a positive but small[8] reactivity step insertion in an infinite, homogeneous reactor that is at the beginning critical at steady state.

The power trend will be featured by a sharp initial increase and it will then adjust to a more slowly increasing tendency. This is due to the fact that, following a reactivity positive step, the multiplication factor is increased and therefore more prompt neutrons are generated instantly[9], giving a sudden increase in neutron concentration.

---

7 Constants A_j can be determined from the reactor's initial conditions.

8 In order to avoid any prompt criticality conditions, the term *small* refers to conditions where the following holds:
$\rho \ll \beta$.

9 This phenomenon is otherwise known as *prompt jump*.

It must be considered, however, that only $(1-\beta)k_\infty$ new prompt neutrons are produced and as long as k_∞ is kept smaller than 1, the reaction is going to be subcritical from a prompt power point of view. This basically means that neutron population growth will fall on a softer trend as the delayed neutrons are emitted.
These results hold for finite reactors as well, where leakage phenomena need to be taken into account.

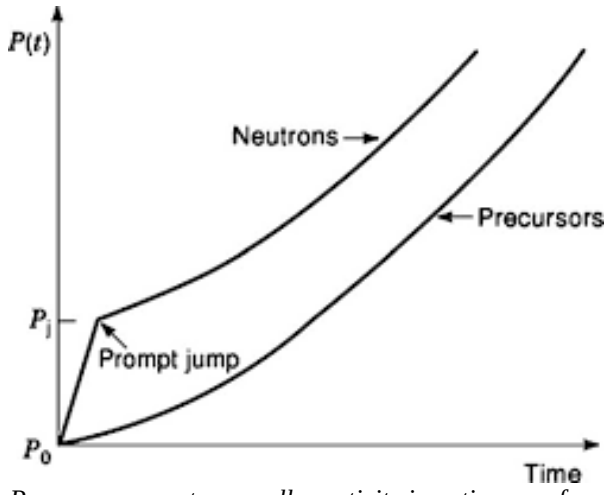

Figure 1.6: Power response to a small reactivity insertion as a function of time.

Chapter 2

Monte Carlo codes

During the last years, high-efficiency computational resources have become more available, leading to a widespread utilization of very effective, though computationally challenging, research tools, such as Monte Carlo codes applied to neutronics.

The birth of Monte Carlo simulation methods is to be traced back to the 1940's, when Stanislaw Ulam was working at the Los Alamos National Laboratory as a member of the Manhattan project (Metropolis and Ulam, 1949). Even though the computational tools at the time were extremely limited, the use of these methods resulted in being fundamental in solving deterministic problems with a probabilistic approach based on random sampling.

For what concerns the field of neutronics, Monte Carlo methods, as opposed to deterministic methods, solve the transport equation relying on the average particle behavior, which is simulated individually and then averaged-out to get a general description, on average indeed, of the whole physical phenomena in the system. Any Monte Carlo based simulation code requires, with their proper input syntax, the following data specifications:

- Geometry description
- Material specifications: it is very important to assign the right cross section to each material in the system, in order to simulate neutron-matter interactions properly
- Locations and features of neutron sources

What these codes effectively do is following a particle along its path, starting from the source until some ending point is reached, such as absorption, leakage, or other terminating events. In other terms, a *particle history* is simulated, which means that the transport equation does not get explicitly solved by the code. This has two main consequences:

1. The number of histories needed to faithfully describe a process is quite large, requiring a sometimes relevant computational expense. Since defining the random samples number as large could be trivial and prone to misinterpretation, it seems useful to proceed further into how accuracy is treated for Monte Carlo simulations. It is out of the scope of this work discussing the mathematical basis behind Monte Carlo methods. Even so, it needs to be specified that, being N the number of simulated neutron histories, accuracy, seen in terms of standard deviation for the simulation output, follows the trend:

$$\sigma \propto \frac{1}{\sqrt{N}}$$

This is very important when considering the precision level at which simulations outputs are requested by the user. If one were to desire, for instance, a reduction in half of the standard deviation associated to the simulation, the number of simulated histories should be quadrupled, at least. Different kinds of errors are present when treating neutronics simulations; other than the one described above, which in general is to be referred to as the *Statistical error*, another very important group is identified as *Systematic errors*. This last type of errors is linked, for the specific case considered here, to the uncertainty around the data used when defining materials for the reactor model. In fact, the data pertaining material concentrations and densities in fresh fuel conditions are intrinsically characterized by uncertainty, which needs to be considered when analyzing results. A further description of this type of errors and on how they have been quantified in the past is present in Chapter 4. However, it is very important to stress how the data currently adopted regarding systematic errors estimate for what concerns reactivity are

just an estimate indeed, as just pointed out, and they are by far the minimum value that can be assessed for systematic uncertainty around reactivity simulation results.

2. Since no transport equation is ever actually solved, there is no need for either geometry, energy, or time approximations. This allows users to apply these simulations to rather complex multi-dimensional, time-dependent problems without compromising accuracy.

Serpent

In this thesis work, the simulation models adopted for the TRIGA Mark II reactor of the University of Pavia were developed by means of the Serpent code.

Serpent is a continuous-energy Monte Carlo reactor physics burnup calculation code (Leppänen *et al.*) and its advantages are related mainly to its computational speed compared to other Monte Carlo codes and to some very useful pre-implemented geometry elements. Its name was originally PSG[10], when the VTT Technical Research Center in Finland started developing it in 2004. The code was eventually pre-released with its current name[11] in October 2008 (Leppänen, 2007).

All the communication between users and the code is handled through one or several input files and different output files respectively. Serpent uses a *universe-based* geometry, where different geometry levels can be found, one nested inside the other. The basis in modeling structures is the *cell*, which is a space domain delimited by simple boundary surfaces and filled with a single homogeneous material, void or another universe. The geometrical advantage provided by Serpent is the pre-implementation of universes (Leppänen, 2013) equivalent to elements that are commonly found in a reactor, such as fuel pins and lattices describing core structures.

Materials need to be suitably defined: each material consists of a number of nuclides, each one with its composition ratio that can be expressed either as atomic or as mass fraction. Each nuclide is then associated with a cross section library, in which there are usually several values for every isotope, depending on the temperature. It is crucial to stress how important it is to consider, for each nuclide, the cross section at the right temperature, in order to appropriately model thermal-motion-related and binding-related effects.

Depending on what the main field of interest for the user is, Serpent gives the possibility of setting calculation parameters to desired values. The most important option regards neutron population and criticality cycles, which as a matter of fact, as

10 Probabilistic Scattering Game.

11 Serpent 1.0.0 at the time.

previously stated, are key in determining accuracy in the results. Serpent can also be run as a burnup calculation code, even though this option was note exploited for the scope of this thesis work.

The main output file provided by the code contains all results calculated by default during transport cycles and other output files might be produced, depending on which options have been set by the user.

Serpent provides users with some advantages with respect to MCNP (Briesmeister, 1986), another widespread Monte Carlo transport code for neutronics. Firstly, Serpent reduces the time required for simulations due to a different approach in modeling particle paths. In particular, MCNP (Team, 2003) adopts *ray-tracing* techniques, which consist in simulating the path and behavior of the particle of interest inside every material of the geometry, which has its own cross section value, and therefore its own interaction probability, starting over at every boundary surface. Serpent, instead, relies on a technique that is called *delta-tracking*, which basically exploits a cross section value which is properly averaged-out between all the materials the particle is going to cross. The approximated cross section is calculated considering also the possibility for the particle of undergoing the so called *virtual collisions*, which do not influence the simulation outcome since neutrons are not absorbed nor lose any energy due to this type of collisions. A path for the neutron is sampled and, without taking into consideration surface boundaries crossings in any way, the kind of collision[12] at the end of the path is sampled as well. This surely introduces some approximations, but it strongly reduces computational expense in terms of time. Serpent is also equipped with built-in burnup methods and, as previously claimed, with pre-implemented geometry elements and universes, which speeds up many modeling processes.

The first model, developed for the TRIGA Mark II reactor fresh fuel configuration and used as a starting base for this work, was built on Serpent 1. For the purposes of this thesis work, Serpent 2 was exploited, which is characterized by some advantages compared to the previous version:

[12] The collision will either be *real* or *virtual*, indeed.

- The memory usage for what concerns cross sections data has been optimized.
- Burnup modules have been optimized.
- The possibility of coupling Serpent 2 with other codes has been introduced. In particular, this allows users to solve multi physics problems such as those treating neutronics along with thermal-hydraulics and thermo-mechanics for instance (Cammi *et al.*, 2011).

Serpent adopts continuous-energy nuclear and atomic data libraries in the Evaluated Nuclear Data File (ENDF) format. As of today, these formats describe nuclear-reaction cross sections, energy distributions, angles of reaction products, nuclei that might be produced, decay modes, decay-product spectra and the estimated errors for all such quantities. All modern nuclear data evaluation work lies in the hands of three main agencies:

- Cross Section Evaluation Working Group (CSEWG) which takes care of the US ENDF/B libraries and the ENDF format. It is coordinated by the National Nuclear Data Center at the Brookhaven National Laboratory.
- JEFF Working Group, whose focus is the European Joint Evaluation Fission and Fusion file (JEFF). Its coordination comes from the Nuclear Energy Agency (NEA) Data Bank which belongs to the Organization for Economic Cooperation and Development (OECD).
- The JNDC, that stands for Japanese Nuclear Data Committee. It handles the Japanese Evaluated Nuclear Data Library (JENDL) and it is coordinated by the Nuclear Data Center at the Japan Atomic Energy Agency (JAEA).

All these organizations group their data adhering to the ENDF format and, thanks to this, Serpent users can freely adopt one of them.

Chapter 3

The TRIGA Mark II reactor

The TRIGA (Training Research and Isotope production General Atomics) Mark II is a pool-type nuclear reactor cooled and partly moderated by light water, with fuel constituted of a mixture of uranium (8%wt and 20%wt-enriched in ^{235}U), hydrogen and zirconium. The reactor was first designed in the early 1950's by General Atomics with the aim of obtaining an inherently safe, research-wise useful and relatively inexpensive reactor. The advantage of this specific fuel composition relays in the presence of a large prompt negative thermal coefficient of reactivity related to the fuel, which means that should the core temperature rise too much, the reactivity would quickly decrease. This feature very much reduces the probability of a core meltdown to occur.

The nominal power is 250 kW when in steady state, while in the past, being the reactor licensed to operate in pulse mode as well, the peak power reached, and kept for a time frame on tens of milliseconds, was around 250 MW.

The reactor is loaded with fuel elements made of uranium and zirconium hydride ZrH_x, where x is the atomic ratio between hydrogen and zirconium, which can vary among different fuel elements.

The tank, which is filled with demineralized water, measures 6,4 m in height and 1,98 m in diameter. The surrounding structure is 6,56 m high and it is made of borated concrete, which plays the role of biological shield. The bottom part is a parallelepiped with basis measuring about 60 m^2 in area and 3,69 m in height. The upper part is an octagonal prism which is 2,87 m high. The core is located 60 cm higher with respect to the bottom of the tank and it is covered by 5 m of water which acts as an effective

biological shield. The core shape is cylindrical, measuring 44,6 m in diameter and delimited by two aluminum grid plates needed for spacing between the fuel elements. On both grids, 90 symmetrical holes can be found, distributed along 6 concentric rings with increasing radius identified as A, B, C, D, E, and F that respectively hold 1, 6, 12, 18, 24 and 30 locations that can be filled either with fuel elements or dummy elements (graphite elements), control rods, or neutron sources. These locations can be alternatively exploited as irradiation channels. A graphite thickness of 30 cm surrounding the core serves as radial reflector, whereas the axial one is provided by two graphite cylinders measuring 10 cm, located at the ends of each fuel rod. Another reflecting contribute is given by light water within the tank itself. In the next two pages three figures can be found: figure 3.1 consists in a picture of the reactor as it appears from the control room. Figure 3.2 and 3.3 contain, respectively, a scheme of the original (fresh fuel) core configuration and the sectional plots for the structure of the TRIGA Mark II of the University of Pavia.

Figure 3.1: The TRIGA Mark II reactor of the University of Pavia

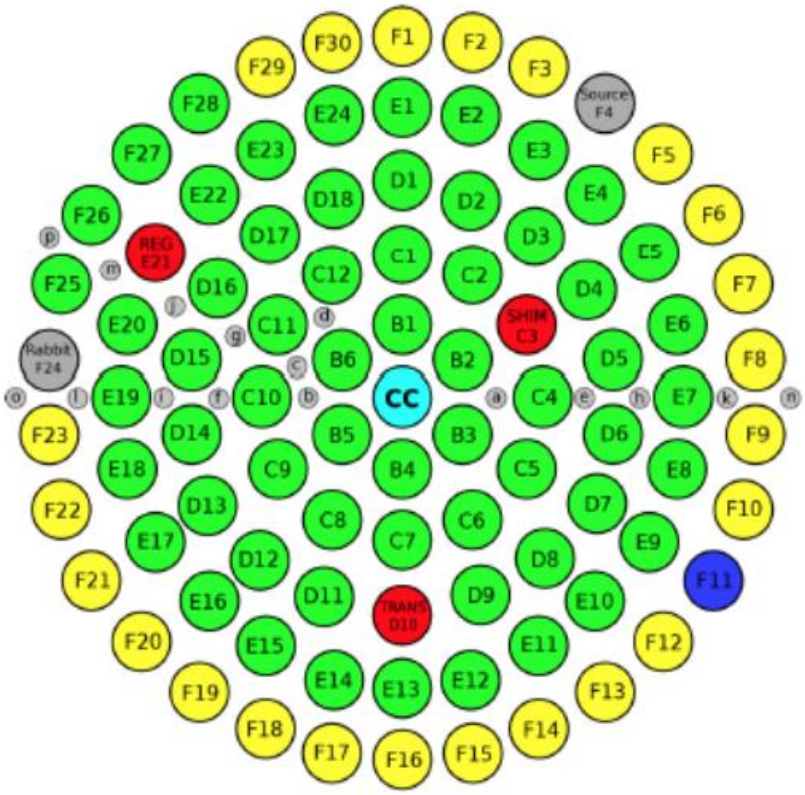

Figure 3.2: Fresh fuel core configuration of the TRIGA Mark II reactor. Fuel elements are (aluminum cladding) are indicated in green, control rods in red, while dummy elements in yellow. The source and irradiating channels are identified with grey and blue.

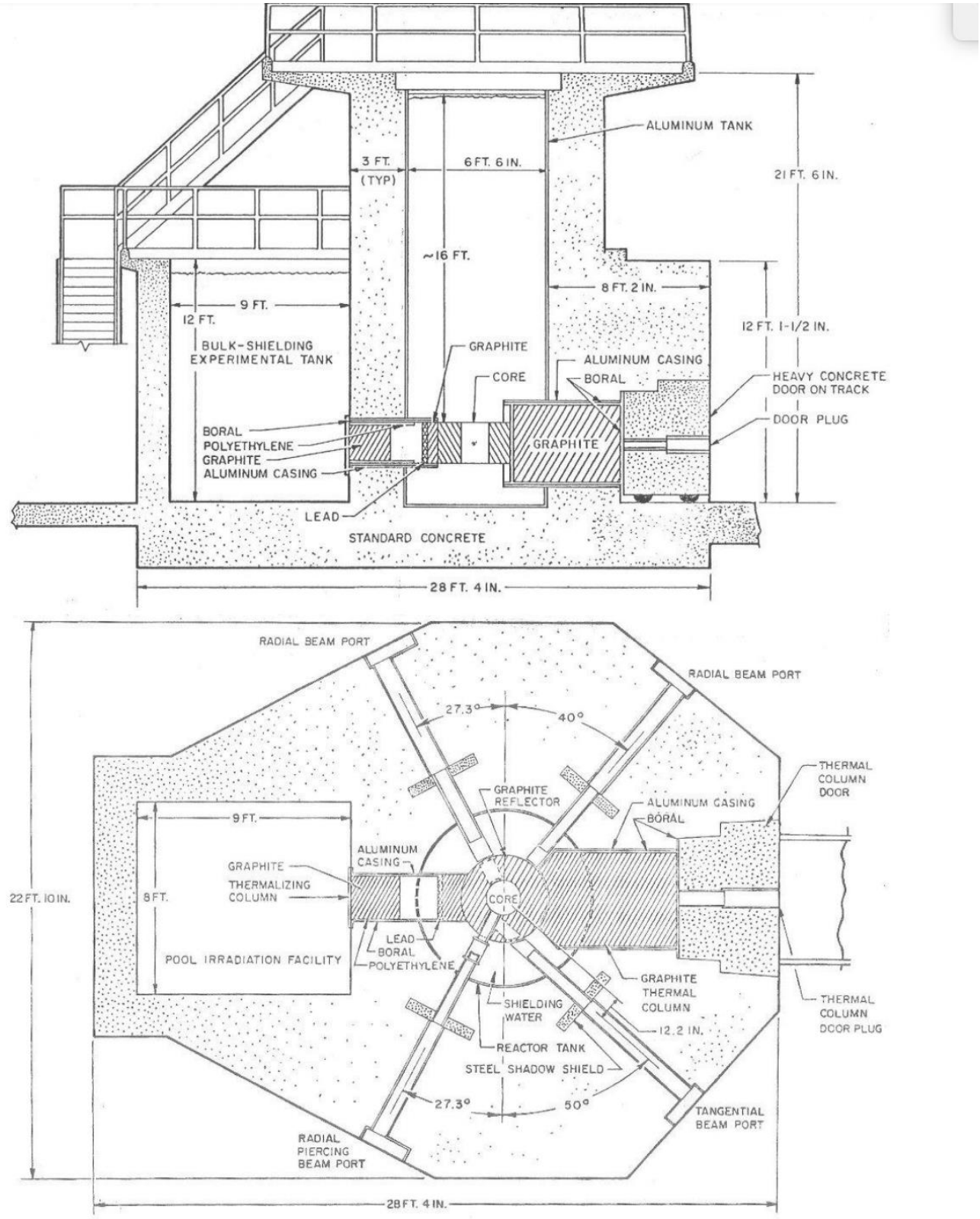

Figure 3.3: Vertical (top) and horizontal (bottom) sections of the reactor.

Fuel Elements

The fuel in this particular reactor, as already stated, contains zirconium hydride, whose moderation effectiveness is inversely proportional to its temperature.

The fuel elements belong to three different manufacturing series that were designed and produced by General Atomics over the years:

- *101-type* which is characterized by the presence of an aluminum cladding and two disks containing Samarium, that acts as a burnable poison. In addition, the atomic ratio between zirconium and hydrogen is 1:1.
- *103-type* in which the cladding is made with stainless steel and there are no burnable poison disks. Here the atomic ration between zirconium and hydrogen is 1:1.6.
- *104-type* with a stainless steel cladding as well and one burnable poison disk characterized by molybdenum. There zirconium to hydrogen ratio is 1:1.6 here as well.

Considering the specific aim of this thesis work, having a good understanding of the different fuel element types structures is of crucial importance in order to faithfully represent the reactor from a model point of view. A graphical representation (not to scale) of the three different structures is presented on the next page, in figure 3.4.

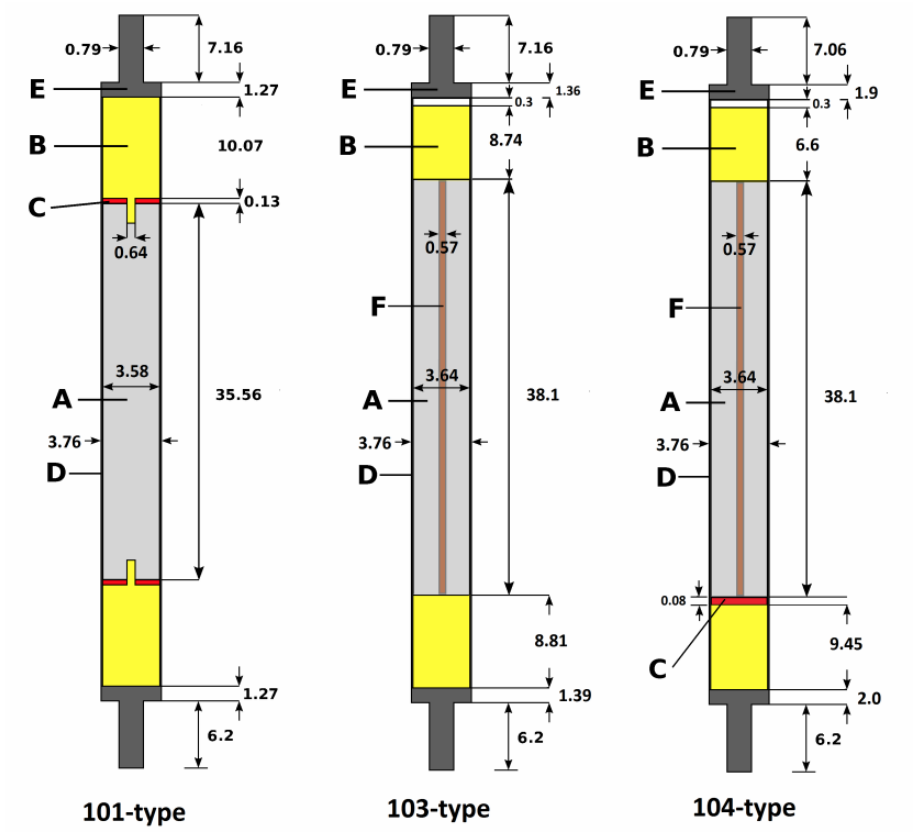

Figure 3.4: Graphic representation (not to scale) of the three different types of fuel elements.

Control Rods

The reactivity control of the TRIGA reactor is carried out through the use of three absorbing rods named Shim, regulating and transient, which during normal operation serve respectively as coarse reactivity adjuster, reactivity criticality tuner and safety rod. They're placed 120 degrees apart taking as reference the core center, which enables operators to obtain a better reactor control by means of symmetrical adjustment of the neutron flux. The shim and regulating control rods are constituted by hot-pressed boron carbide (B_4C) powder, whereas the transient one is a solid graphite rod with 25%wt free boron.

Each control rod is enclosed in an aluminum cladding connected to a mechanism which allows to move the rod at the velocity of 29 cm/min along a guide tube. An

additional anchoring electromagnetic system allows the control rod quick release in order to obtain rapid reactor shutdown in need of a scram or in case of a plant black out.

The extraction path followed by all three control rods is measured in *step units*[13] and they are characterized by the following features:

- The regulating control rod covers a distance of 38,1 cm going from step 116 to step 821, thus performing 705 steps.
- The shim control rod covers the same distance as the regulating one, with the same number of steps. The only difference is the starting and ending steps, which are 130 and 835 respectively.
- The transient control rod spans a distance of 47,2 cm with 873 steps from step 53 to step 926.

It is worth to mention that the most important role in compromising, as one might say, modeling efforts, is played by the transient control rod, since manufacturing information pertaining this reactor element are the ones characterized by the least precise data.

[13] A step unit equals about 0,054 cm.

The new model of the TRIGA Mark II reactor

The main goal of this thesis work is to develop a Serpent model adherent to the reactor contemporary conditions in terms of geometry and material composition. The main purpose of this model would have then been the Monte Carlo calibration of one of the control rods and a partial calibration of another control rod. The starting point was an already-existent and experimentally validated model for the reactor fresh fuel configuration referred to 1965 first criticality condition (Castagna *et al.*, 2018). The code adopted in this specific work was Serpent 1. In particular, this model was built upon historical data collected at LENA (Cambieri *et al.*, 1965) and provided by General Atomics. The cross sections adopted are taken from JEFF-3.1 library (Santamarina *et al.*, 2009) and ENDF/B-VII.1 library (Chadwick *et al.*, 2011) for what concerns $S(\alpha,\beta)$ cross sections. In this work, the core is modeled defining a circular cluster array, which is a pre-implemented geometrical structure available in Serpent which enables users to describe the 91 core locations distributed along concentric rings. These locations are filled with fuel elements, control rods, graphite elements (also known as *dummy*), the neutron source and the two irradiation facilities (*Central Thimble* and *Rabbit Channel*). The fuel elements are modeled in detail, since a different material was defined for each fuel element, in order to be as close as possible to the actual uranium content in each element exploited at the beginning of reactor operation in 1965. This configuration was characterized by the presence of a single type of fuel rod (in particular, the 101-type described previously), a particular core configuration and by the presence of water in the central channel. A radial and transversal plot obtained through Serpent simulations are displayed in the next page to have a better insight on how the fresh fuel configuration has been modeled.

As the years went by, the core configuration slightly changed and two additional fuel rod types provided by General Atomics (103 and 104-type) started to be employed in the reactor.

The first step of this work has been, in order to acquire confidence with Serpent and the model itself, performing some simulations regarding fresh fuel configuration with Serpent 2. To this purpose, twenty-six criticality configurations at fresh fuel were

reproduced using Serpent 2 and exploiting the available model (Castagna *et al.*, 2018). All the configurations refer to criticality in low power conditions, which means that thermal-related feedback effects do not play any significant role in influencing reactor behavior. The results in term of reactivity for all twenty-six configurations are shown in table 3.5 and in figure 3.6.

Configuration Number	**Regulating CR position** [cm]	**Shim CR position** [cm]	**Transient CR position** [cm]	**Reactivity** [pcm]	
1	20,89	23,00	20,52	62 ± 7	
2	17,49	24,3	20,52	74 ± 7	
3	29,59	27,27	0	215 ± 7	**Mean**
4	25,70	28,73	0	178 ± 7	
5	22,19	30,89	0	180 ± 7	165,2 pcm
6	19,06	33,59	0	215 ± 7	
7	16,85	38,07	0	231 ± 7	
8	38,07	13,82	out	312 ± 7	
9	28,57	15,12	out	213 ± 7	
10	23,92	16,52	out	140 ± 7	
11	19,66	17,93	out	130 ± 7	
12	16,25	19,17	out	91 ± 7	
13	12,31	20,57	out	88 ± 7	**Standard Deviation**
14	7,78	21,82	out	124 ± 7	
15	0	23,00	out	129 ± 7	
16	out	25,76	0	193 ± 7	73,6 pcm
17	out	24,46	5,24	212 ± 7	
18	out	23,33	9,02	98 ± 7	
19	out	21,87	13,34	48 ± 7	
20	out	20,14	17,66	65 ± 7	
21	out	18,68	21,98	89 ± 7	
22	out	17,12	26,29	153 ± 7	
23	out	15,93	30,62	192 ± 7	
24	out	15,49	32,78	252 ± 7	
25	out	14,74	36,02	275 ± 7	
26	out	14,20	39,26	250 ± 7	

Table 3.5: Reactivity output values expressed in pcm for the criticality configurations at low power referred to fresh fuel conditions obtained with Serpent, along with their mean and standard deviation.

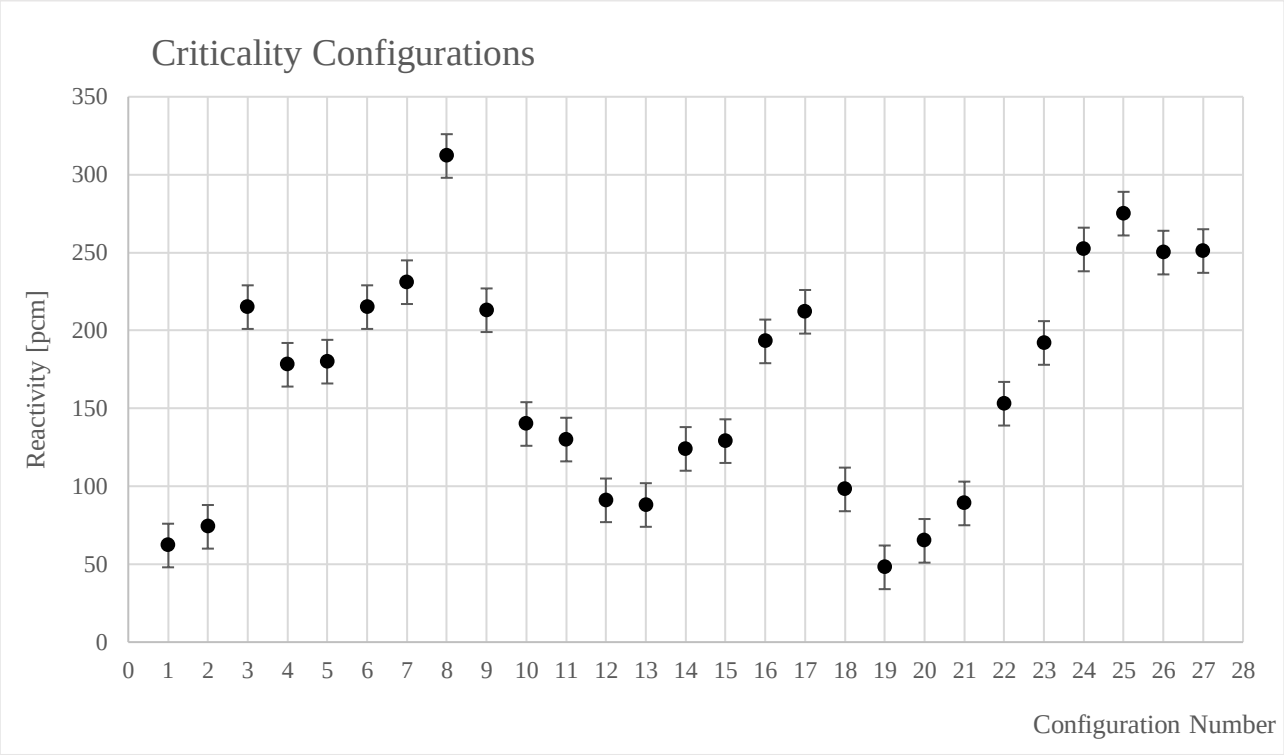

Figure 3.6: Reactivity values in pcm for the criticality configurations at low power referred to fresh fuel conditions simulated with Serpent.

When analyzing data pertaining simulations output, it needs to be taken into account that three main different error sources are to be considered. The first one is the one already described in Chapter 2, related to the Monte Carlo method itself, that can be referred to as *statistical Monte Carlo uncertainty*. Another term of uncertainty is directly linked to the so called *systematic errors*, which will be further described, for this reactor, in the next chapter. The important aspect to focus on is the fact that systematic-errors-related uncertainty depends on the specific case and it requires detailed sensitivity studies in order to be assessed (Alloni *et al.*, 2014). What is worth to mention in this section is that for the TRIGA Mark II considered in this work, the estimate for the minimum systematic errors uncertainty source is around 190 pcm (Alloni *et al.*, 2014). The last main term of uncertainty can be obtained performing a statistical analysis of the dataset of interest and computing the standard deviation, which has been done in this case, as it can be seen from table 3.5. For all the configurations included in table 3.5 and figure 3.6, experimental criticality is correctly reproduced taking into consideration as uncertainty both the statistical one

related to the whole dataset trend and the one related to systematic errors, which is a good result in terms of model validity.

After testing the reactor model with Serpent 2, the actual update in order to correctly reproduce current reactor conditions started with the retrieval of information pertaining fuel material data.

From a previous study, a burnup analysis of a previous work with MCNP (Chiesa *et al.*, 2016; Chiesa, 2014) for the reactor was performed via MCNP simulations and an optimized core reconfiguration was conceived and completed on September 25, 2013. There was therefore the need to update the Serpent model in order for it to be as similar as possible to the reactor as it is nowadays, in order to make it suitable for reactor analysis in the present configuration. The differences, other than the fuel elements exact positions inside the core, between the fresh-fuel condition and the current one are mainly three:

- The three different fuel rod types.
- The central channel has now been emptied.
- The materials have undergone depletion processes through irradiation.

All these elements needed to be accounted for while updating the model. For what concerns the third point, data coming from MCNP fuel burnup calculations (Chiesa, 2014) and referring to September 9, 2013, were exploited and adapted into a feasible Serpent input file. The burnup results were available for uranium pins and for burnable poison disks (Molybdenum, Samarium) as well as for each fuel element, which made it possible to keep the same detail level adopted in the original model. Definitions for the 103-type and 104-type fuel rods (see figure 3.4) were introduced and the central channel was filled with air. The original model was featured by a burnable poison definition that was standardized for every fuel rod and had to be changed since the depletion data were available for every distinct fuel element. In order to define distinct Samarium and Molybdenum disks, new single pin universes (that are standard pre-implemented universes available in Serpent) were added for each fuel element containing materials defined solely for that precise fuel element. The lattice configuration was then modified exploiting the data belonging to the documentation available, which were adherent to the up-to-date configuration.

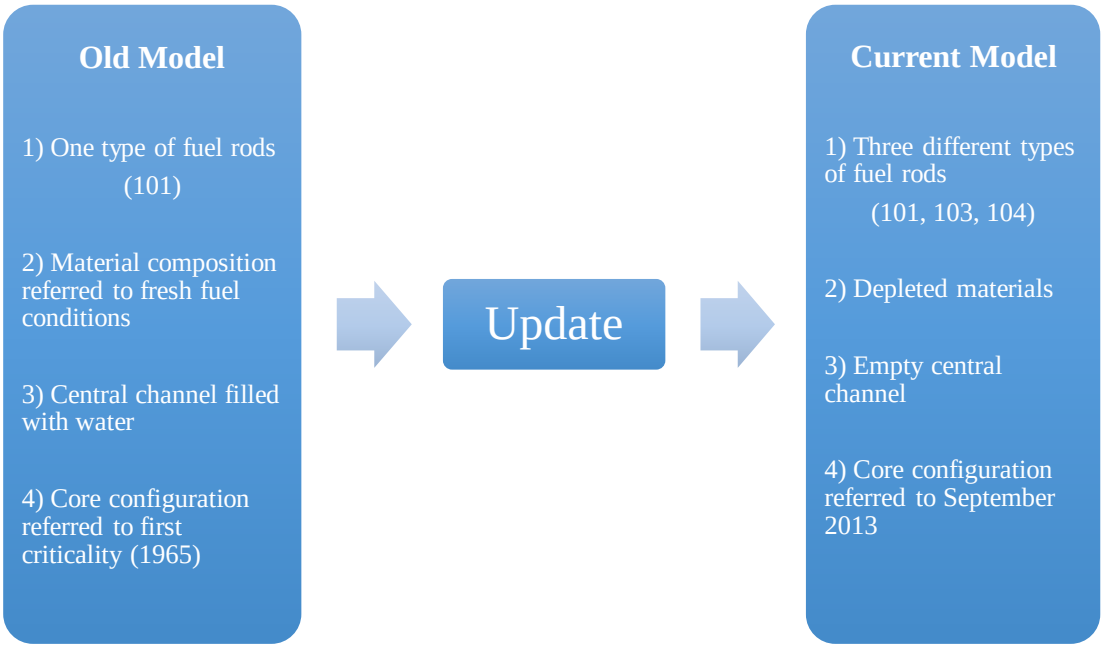

Figure 3.7: Schematic view of the model referred to 1965 conditions versus the one referred to 2013 conditions.

All the cross sections employed in this frame were pre generated by means of the MAKXSF utility (Brown, 2006) at 10K temperature intervals. When considering low power conditions, meaning that the power produced is below 10W, the reactor can be assumed in thermal equilibrium with the external environment. The overall reactor thermal condition was therefore approximated to be at 300K and all the cross sections considered are referred to this temperature. This stands for both moderator and fuel cross sections.

When simulating reactor behavior at full power, the cross sections employed had to be referred to the proper working temperature in order to correctly assess the thermal phenomena and effects regarding neutron-matter interactions, for what concerns both fuel and moderator. Temperature distributions for the fuel were therefore adopted in order to correctly select all the cross sections and in order to consider all temperature related phenomena. For what concerns temperature distributions (figure 3.8), data coming from an analysis performed coupling COMSOL (https://www.comsol.it/) and MCNP softwares (Cammi *et al.*, 2016), that had subsequently undergone experimental validation, were exploited.

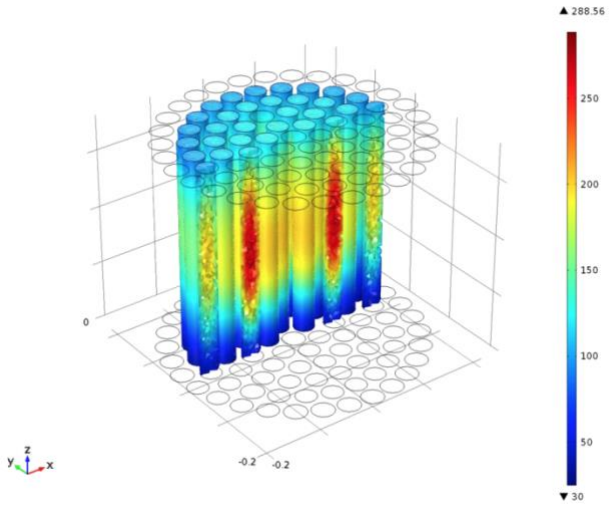

Figure 3.8: Fuel elements temperature distribution in ℃ at full power.

In fact, as stated in previous chapters, the core is organized in concentrical rings in which each element can be furtherly subdivided into five vertical sections (see table 3.9) for which a specific temperature has been identified, in order to approximate, with acceptable accuracy, the continuous temperature distribution. These data have been implemented into Serpent materials scripts in order to faithfully reproduce the reactor's response at full power and taking into account the fact that the cross sections libraries provide values at 10 K intervals, which means that some values had to be rounded up.

	Core Ring				
Fuel Section	**B**	**C**	**D**	**E**	**F**
1	430	420	410	390	380
2	490	480	460	430	400
3	500	500	480	430	400
4	480	460	440	400	370
5	370	360	350	360	330

Table 3.9: Temperature values in Kelvin at full power for each vertical section of each core ring.

All the information and features available for what concerns current reactor geometry state and the different aspects to be considered regarding different operating

conditions were included in performing the model update in a format which would be suitable for the Serpent 2 code version.

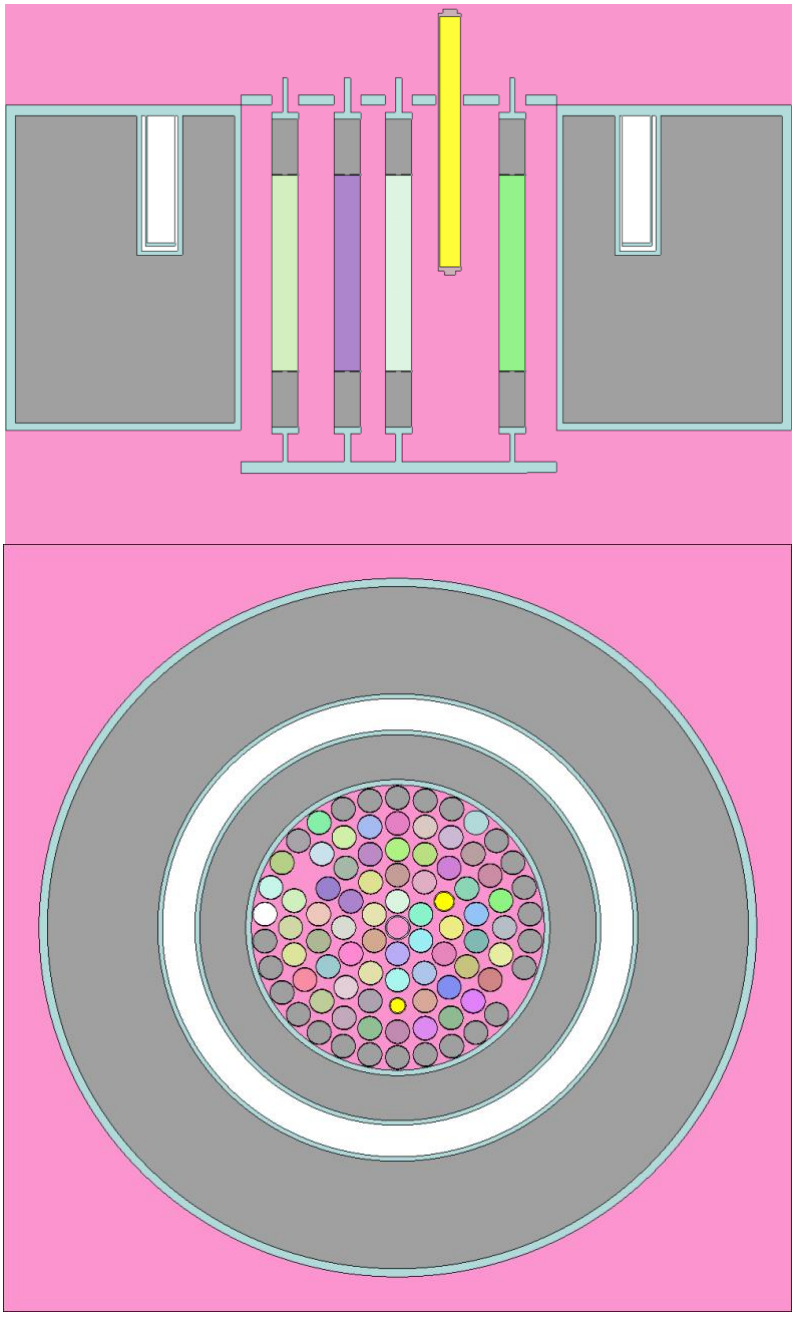

Figure 3.10: Vertical (top) and radial (bottom) sections of reactor geometry plotted with Serpent 2 for the fresh fuel model.

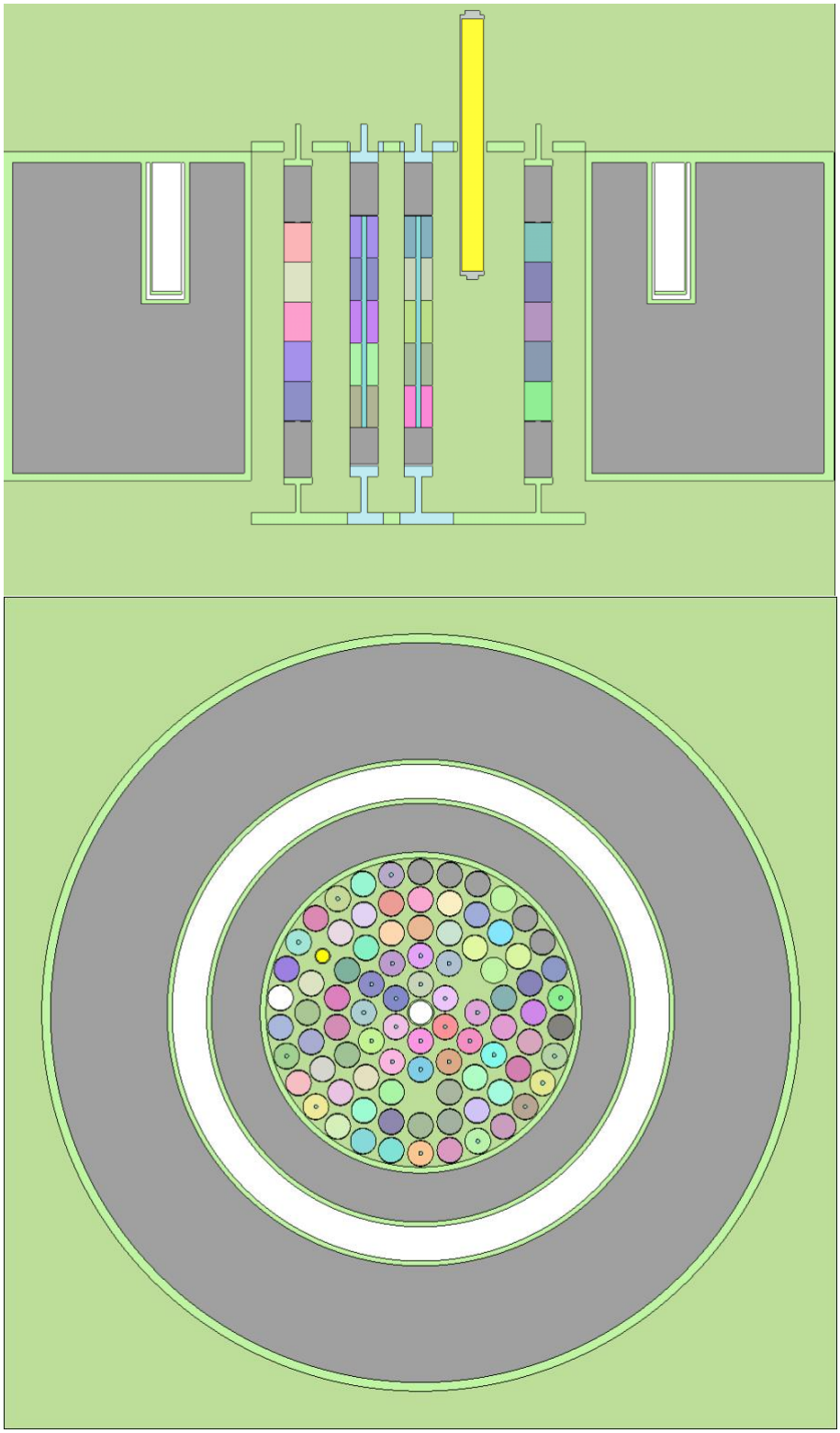

Figure 3.11: Vertical (top) and radial (bottom) sections of reactor geometry plotted with Serpent 2 for the updated model.

In figure 3.10 and in figure 3.11 the plotted geometries for the Serpent 2 model referred to fresh fuel and current reactor conditions, respectively, are shown. For the sake of simplicity, the geometry shown in figure 3.10 is based on the model suitable for low power criticality simulations, thus no vertical fuel distinction is present, since no temperature distribution is taken into consideration when reproducing low power criticality conditions, as previously explained. Plot colors are not indicative of the type of material; they have been selected to make different geometry parts clearly distinguishable. The burnable poisons disks cannot be noticed from these plots, being them extremely thin, even though they have been included in the model; the inner zirconium cylinder, present in 103 and 104-type fuel elements can be observed in figure 3.11, both in the radial and vertical sections. What needs to be stressed about the process that led to the update of the TRIGA Mark II reactor model is that the crucial part, other than geometry specifications, that influenced accuracy in this work, was material definition. The crucial part of this work was indeed including all the data available from burnup calculations into the material definitions for the reactor in order to correctly simulate its behavior from a neutronics point of view.

Chapter 4

Results of the Update

In order for the updated model to be validated, the first configuration explored was the one pertaining the first full power criticality reached in 2013 after core reconfiguration.

The reactivity has been computed taking the k_{eff} value provided as output from the simulation and applying the following: $\rho = \frac{k_{eff}-1}{k_{eff}}$ [14] and expressing it in pcm.

In performing simulations, there are three key factors that need to be set in the input file that users provide Serpent with and that determine the statistical accuracy of the simulation. The first parameter to be introduced is the number of *inactive cycles*, which are the ones needed in order to allow the initial fission source distribution to converge before starting to collect the results. Serpent manual suggests users to set at least 20 inactive cycles, but in full-core calculations convergence may take more cycles to be reached. For the simulations exploited in this thesis work, the number of inactive cycles was set to 100. The other two factors are, respectively, the *population size per cycle* and the *number of active cycles* for the simulation. The statistical accuracy of the results depends on the total number of neutron histories run, therefore on the product of the two parameters just introduced, as explained in Chapter 2. The typical value for population size and number of cycles, respectively, for lattice calculations suggested by Serpent manual is 5000 and 500. As the geometry increases

[14] The k_{eff} value is the multiplication factor value considering leakages and absorptions, thus in a non-ideal, finite reactor.

and accuracy requirements become more stringent, it is necessary to increase such quantities, compatibly with computational availability (Leppänen, 2013).

All the simulations performed for this thesis work are characterized by 8000 cycles with 40000 neutrons each. The uncertainty around the output reactivity resulted $7\ pcm$ for each simulation.

Considering thermal effects on both fuel and moderator and consequently adjusting the material definition, the simulation provided an output reactivity value of $1{,}99996\ pcm \pm 7\ pcm$[15], in agreement with experimental values.

A very important role in determining the accuracy of the simulation is played by the so called *systematic errors*, which must be evaluated. For what concerns this particular reactor, the previously defined errors have been quantified in (Alloni *et al.*, 2014) as around $190\ pcm$ by propagating uncertainties related to fuel enrichment and graphite density data. It needs to be specified that, since these data have undergone burnup calculations, which have been executed via Monte Carlo codes characterized by uncertainty themselves, a further error propagation might be hypothesized. On this basis, the assumption regarding simulation outputs uncertainty should be that, apart from the Monte Carlo statistical uncertainty, which is around $7\ pcm$, one should expect another uncertainty term related to systematic errors whose value can be inferred to be at least $190\ pcm$. The important feature that always needs to be taken into account regarding systematic errors is related to the fact that the value just expressed is the *minimum* value for systematic errors that can be considered. This stands for all the results considered in this work.

In order to obtain a further validation for the updated model, a simulation aimed at obtaining as a result the core excess was performed simulating the reactor in low power conditions. The core excess for a reactor can be defined as the reactivity value pertaining the retrieval of all control rods from the core. The reactivity obtained with Serpent was compared with the one obtained through MCNP simulations and experimental procedures (Chiesa, 2014).

[15] The value of $7\ pcm$ is the statistical error associated to the Monte Carlo simulation.

Experimental **Core Excess** [pcm]	**MCNP** **Core Excess** [pcm]	**Serpent** **Core Excess** [pcm]
$1817{,}7 \pm 21{,}9$	$1919{,}9 \pm 36{,}5$	$2016{,}5 \pm 7$

Table 4.1: Core Excess values expressed in pcm from experiments, MCNP and Serpent.

As it can be noted from table 4.1, the results obtained through Serpent simulations in terms of reactivity appear to be compatible with experimental and MCNP results within a 2σ interval, considering systematic uncertainty.

In addition to the previously shown results, criticality configurations at low power were simulated and compared to experimental benchmarks obtained when experimentally calibrating control rods. Criticality configurations were experimentally achieved in two different moments; this means that there is the availability of two different datasets. The first one has been collected in 2015 and the second one in 2018 and they refer to different control rods position. For the former dataset, eight criticality configurations were reproduced, while for what concerns the latter, it consists of six criticality configurations. During experimental procedures, the transient control rod was kept extracted at all times and therefore the simulated geometries followed this condition. Both datasets were reproduced using the updated model via Serpent and a statistical analysis was conducted in order to investigate the general behavior of the simulated output data.

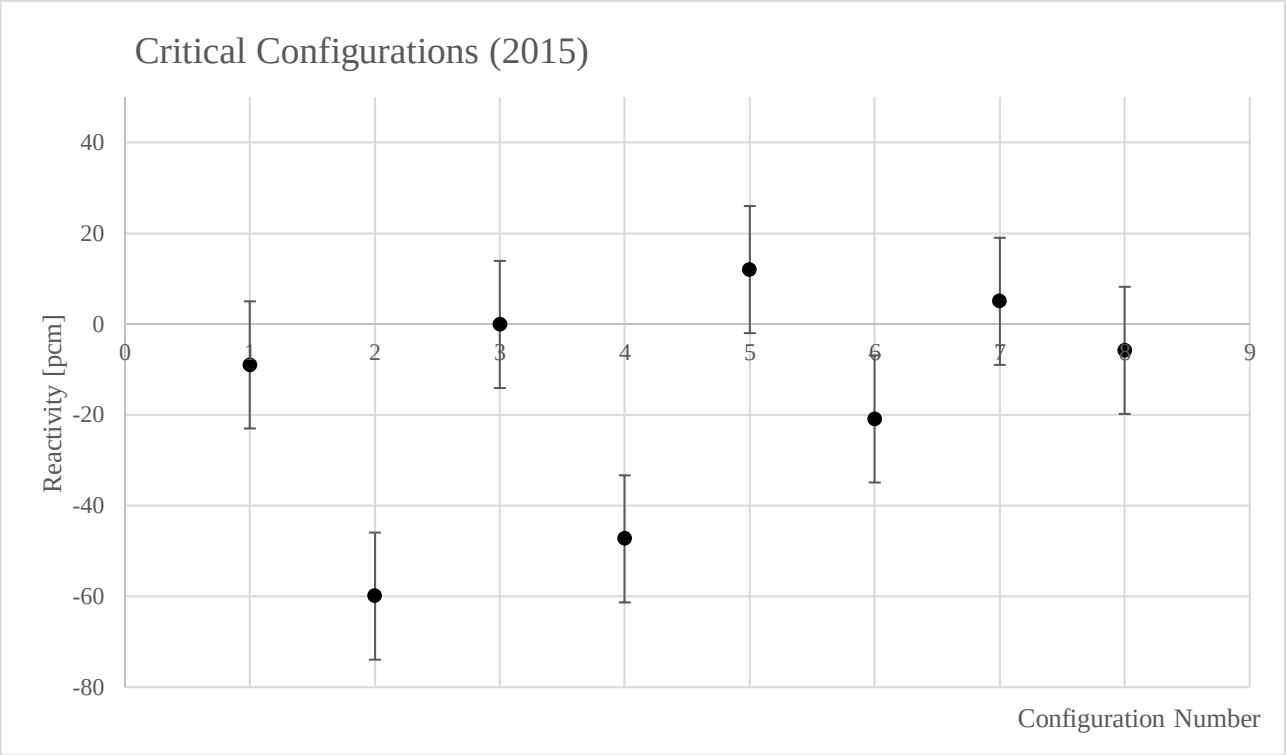

Figure 4.2: Reactivity values in pcm for the different criticality configurations (2015) simulated with Serpent.

Configuration Number	**Regulating CR position** [cm]	**SHIM CR position** [cm]	**Reactivity** [pcm]	
1	0,27	19,92	-9,00 ± 7	
2	4,57	19,38	-59,93 ± 7	
3	9,85	8,45	-0,1 ± 7	**Mean** -15,76 pcm
4	13,77	16,93	-47,32 ± 7	
5	17,69	15,51	11,99 ± 7	
6	21,55	13,93	-20,90 ± 7	**Standard Deviation** 25,54 pcm
7	24,77	12,74	4,99 ± 7	
8	27,21	11,81	-5,80 ± 7	

Table 4.3: Reactivity values in pcm for the different criticality configurations (2015), with the mean and standard deviation for the Serpent output dataset.

As it can be observed from the values reported both on figure 4.2 and on table 4.3, the reactivity values obtained for configuration 1, 3, 5, 7 and 8 appear to be in agreement with experimental criticality within a 2σ interval, without taking into account systematic errors, but just considering Monte Carlo statistical uncertainty. For what concerns configurations 2, 4 and 6, if systematic uncertainties are taken into consideration as well, the agreement with experimental criticality can be found within 1σ. Considering the mean and standard deviation for the dataset as a whole, experimental criticality reproduction is correctly reproduced in 1σ, as one can see from table 4.3.

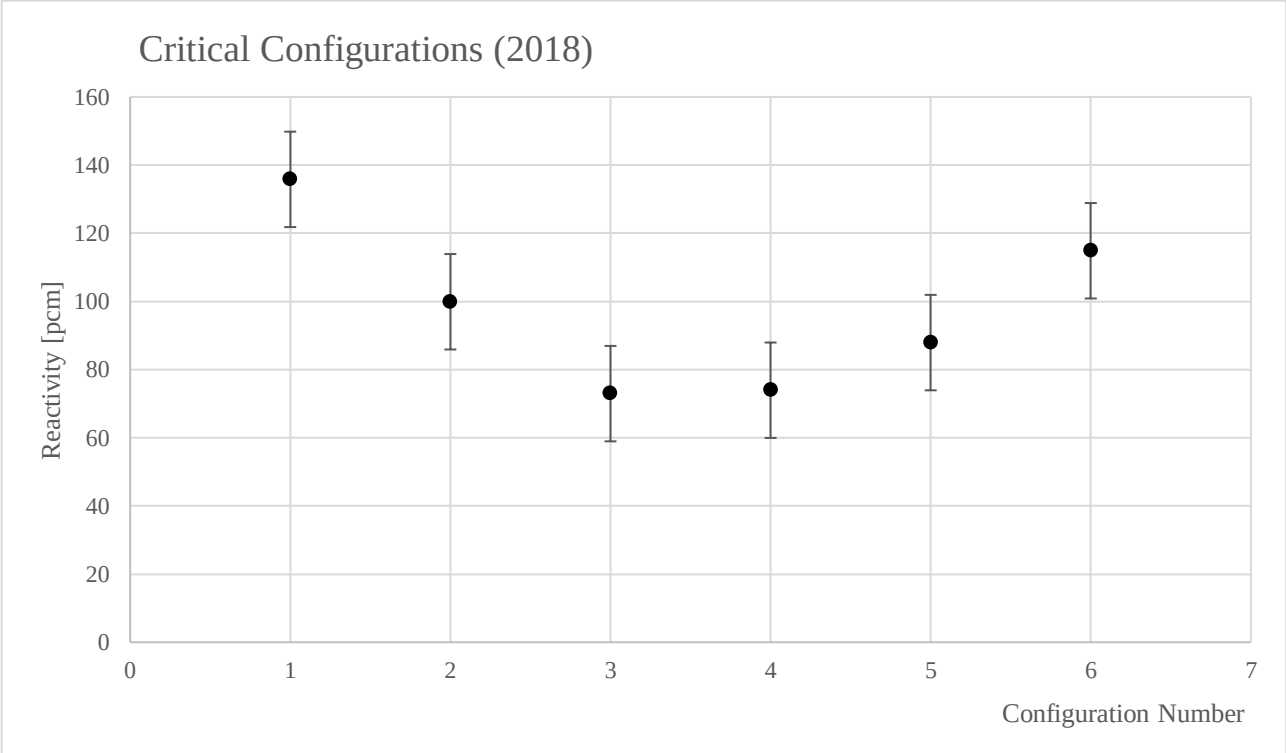

Figure 4.4: Reactivity values in pcm for the different criticality configurations (2018) simulated with Serpent.

Configuration Number	**Regulating CR position** [cm]	**SHIM CR position** [cm]	**Reactivity** [pcm]	
1	0	21,67	$135{,}81 \pm 7$	**Mean** 97,57 pcm **Standard Deviation** 24,59 pcm
2	9,24	19,99	$99{,}90 \pm 7$	
3	14,65	17,99	$72{,}95 \pm 7$	
4	18,91	16,53	$73{,}94 \pm 7$	
5	23,45	14,86	$87{,}92 \pm 7$	
6	28,81	12,97	$114{,}87 \pm 7$	

Table 4.5: Reactivity values in pcm for the different criticality configurations (2018), with the mean and standard deviation for the Serpent output dataset.

It is can be observed, above all from table 4.5, that 2018 simulation results are affected by a constant offset which can be related to the fact that the material definitions exploited in the updated Serpent model are based on burnup output data referred to September 2013. Materials within the reactor have indeed undergone irradiation and therefore further burnup between 2013 and 2018, which means that the values reported above, regarding 2018 criticality configurations, provide an overestimation of the system reactivity. In addition to this, it needs to be specified that, at the moment in which the experimental procedures were performed, the reactor was in an equilibrium condition for what concerns the presence of poisons. In order to consider this last aspect, an optional setting regarding poison equilibrium was included in the input files exploited to reproduce these configurations. All the configurations appear to be supercritical and the mean value for the whole dataset results in being supercritical as well. Analyzing the dataset considering also the influence of systematic uncertainties, it can be stated that every configuration simulation output and their mean are in agreement with experimental criticality within 1σ.

Two experimental data sets, collected in order to perform the regulating rod calibration, were exploited and taken as a reference in order to compare simulations results. The reactivity values were obtained exploiting the reactor stable period method, which will be briefly presented, alongside the experimental techniques adopted, in the next pages.

Experimental Datasets Collection

In this paragraph, the experimental procedures performed in order to collect the data needed as a comparison reference for Monte Carlo simulations will be described.
The main purpose of these procedure is to empirically, through the use of the *reactor stable period method*, the Regulating control rod and partly calibrate the Shim control rod as well, taking advantage of its role in restoring reactor criticality.
The main parameter measured during this experiment is the *time* required to obtain a power increase; this is basically achieved using different chronometers.
In order to always have power levels under control three different instruments are available on site:

- *NLW-1000*: it is a wide-range logarithmic channel that combines the functions of logarithmic counting and logarithmic current conversion. It provides a continuous indication of reactor power from source level to full power and it is connected to a fission chamber.
- *NMP-1000*: it is a wide-range, analog linear current mode module with range-switching. Ranges may be selected either manually or automatically, locally or remotely. It takes as input the signal provided by an ionization chamber.
- *NP-1000*: it is an analog neutron-monitoring safety channel with an additional local digital display. It uses signals from self-powered in-core detectors or ionization chambers. It may also be used to monitor temperature or other parameters. Its output signal integrity is assured by the presence of isolation devices and input signals as low as 10^{-9}A to 10^{-3}A are feasible. Gain adjustment is manual and range selection can be done either manually or via computer.

The experiment is carried out keeping the Transient CR extracted at all times, while adjusting the position of the other two rods.
In order to properly calibrate the control rods, the power is always kept below 10W, in a so called *Zero power condition*, because it is necessary not to have any thermal feed backs interfering with the measurement results.

The regulating control rod is initially completely inserted into the core and the Shim CR is brought in such a position to obtain criticality at the power of 1W. Once the reactor is set as critical, the regulating control rod is extracted in order to achieve super criticality. Being the reactivity positive, the power will start rising and the time required to shift from 3W to 4,5W and subsequently from 4,5W to 6W (therefore two 1,5 relative escalations) are registered via different timers. Once the data necessary to compute the reactor period have been recorded, an adjustment in the Shim's position is performed in order to restore criticality.

The previously described steps are then repeated until complete extraction of the regulating control rod is obtained. Since at each step, the Shim is then inserted to bring the reactor back to criticality, it is also possible to say that the negative reactivity injected through the Shim to counterbalance the regulating control rod extraction effect is equal and opposite to the positive reactivity insertion obtained through the regulating control rod insertion. The data sets adopted in this thesis were two different ones, the first one collected in 2015 and the second one during fall 2018. For the latter data set, the experiments were performed in the afternoon and the reactor had been operated at full power for several hours on the same day in the morning. When analyzing such data and comparing them to simulations, it needs to be taken into account that poisons such as Xenon were present while conducting experimental procedures, which led to the adoption of different control rods positions (slightly more extracted, compared to the equivalent ones adopted in 2015) in order to reach criticality. For what concerns the 2018 dataset, it is also to be taken into account the reactor has been operated for three years and some burnup effects, even if not quantifiable, will be present.

For what concerns the physical properties behind this procedure, as explained in higher detail in Chapter 1, when introducing a positive step of reactivity, the power trend can be expressed also as follows:

$$P(t) = P(0)e^{\frac{t}{T}}$$

where T is defined as the *reactor period*, $P(t)$ is the power value at time t and $P(0)$ is the initial power condition. The reactor period is therefore the time required by

power to increase by a factor e. In the case analyzed, only power increases of 1,5 have been treated.

The reactor period can be then obtained as:

$$T = \frac{t_m}{\ln(1{,}5)}$$

where t_m is the experimentally measured time required to obtain a 1,5 power escalation.

The reactivity corresponding to the measured period can be retrieved exploiting the Inhour equation in the following form:

$$\rho = \frac{\Lambda}{T} + \sum_{i=1}^{6} \frac{\beta_i}{1 + \lambda_i T}$$

where Λ is the *mean generation time*, whose value has been taken as $50\ \mu s\ \pm 10\ \mu s$. β_i and λ_i are, respectively, the i-th delayed neutron fraction to total neutron population and precursor decay constant for each delayed neutron group.

The trend of the reactor period as a function of reactivity insertion expressed in dollars can be observed in figure 4.6. Different trends can be found depending on the value of Λ.

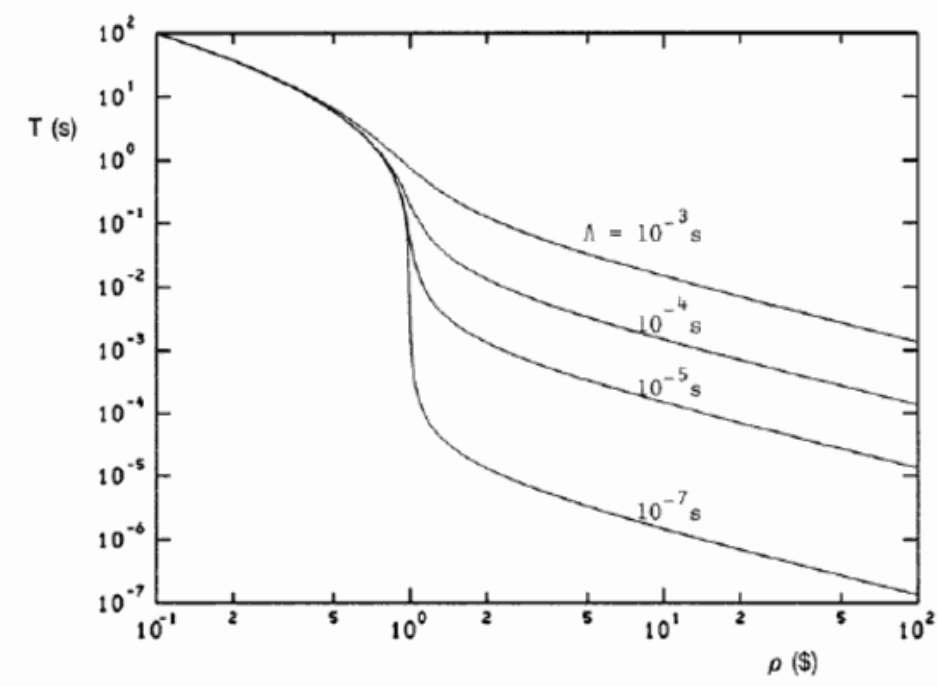

Figure 4.6: Reactor period trends expressed in seconds as a function of reactivity, expressed in dollars, and of the mean generation time.

Considering uncertainty around the computed reactivity value, the technique proposed by Robert J. Moffat (Moffat, 1988) to account for uncertainty on a calculated output of the different uncertainty contributions provided by the considered inputs, was adopted. When dealing with an output whose uncertainty is still unknown, all the inputs x_i related to that particular output and that are known the uncertainties on, need to be considered.

Labeling as δ_i the error on the i-th input, an upper and lower bound for that input variable can be expressed as:

$$U_i = x_i + \delta_i$$

$$L_i = x_i - \delta_i$$

Considering now the uncertainty ε related to the output quantity, it can be computed as:

$$\varepsilon = \sqrt{\sum_{i=1}^{N} \left(\frac{|U_i| - |L_i|}{2} \right)^2}$$

where N is the number of input variables needed to compute the final quantity.

The parameters whose uncertainty needs to be known in order to compute the overall uncertainty around experimental reactivity are the mean generation time Λ, the six delayed neutron fractions and precursors decay constants and the reactor period collected experimentally. In this particular frame, it can be exploited another expression for the Inhour equation, which is the following:

$$\rho = \frac{\Lambda}{T} + \beta \sum_{i=1}^{6} \frac{f_i}{1 + \lambda_i T}$$

Where β is the total fraction of delayed neutrons to total neutron population, constituted by the sum of the fractions of delayed neutrons to total neutron population for each group:

$$\beta = \sum_{i=1}^{6} \beta_i = 730\ pcm\ \pm 35\ pcm$$

The quantity f_i is then defined as the fraction of delayed neutrons belonging to the i-th group to total delayed neutron population:

$$f_i = \frac{\beta_i}{\beta}$$

The values for f_i and λ_i for all six groups are collected in the following table:

f_i	λ_i [s-1]
0,042 ± 0,008	3,01 ± 0,33
0,115 ± 0,009	1,14 ± 0,15
0,395 ± 0,011	0,301 ± 0,012
0,196 ± 0,022	0,111 ± 0,004
0,219 ± 0,009	0,0305 ± 0,0001
0,033 ± 0,003	0,0124 ± 0,00003

Table 4.7: Fractions of delayed neutrons to total delayed neutron population and precursors decay constants for each delayed neutron group, along with uncertainties.

As already mentioned, the value for the mean generation time is:

$$\Lambda = 50\ \mu s\ \pm 10\ \mu s$$

Two experimental datasets exploited as a reference tool for simulations outputs were collected respectively in 2015 and 2018. For both of them, the uncertainty around the value of the reactor period was obtained through the standard deviation of the measured values. In particular, for each calibration point fifteen values for the reactor period were measured. For each calibration point, reactivity was computed through the Inhour equation from both a differential and an integral perspective. Subsequently, uncertainties on all the parameters listed above were combined using the technique proposed by Moffat in order to obtain the uncertainty around reactivity.

In table 4.8 and 4.9 are listed the configurations for the control rods, along with the measured reactor period T, integral and differential reactivity. The position for the control rods takes as reference their complete insertion.

Shim CR position [cm]	Reg. CR position [cm]	T [s]	Δρ [pcm]	ρ [pcm]
19,92	0,27	∞	0	0
19,92	4,57	194,15 ±3,13	41,79 ± 3,49	41,79 ± 3,49
19,38	9,85	58,48 ± 0,81	107,42 ± 8,37	149,21 ± 9,07
18,45	13,77	40,89 ± 0,59	136,64 ± 10,65	285,84 ± 13,99
16,93	17,69	45,13 ± 0,59	128,12 ± 9,97	413,96 ± 17,18
15,51	21,55	40,74 ± 0,64	136,96 ± 10,69	550,92 ± 20,23
13,93	24,77	59,56 ± 0,81	106,04 ± 8,26	656,95 ± 20,84
12,74	27,21	86,15 ± 0,32	80,94 ± 6,26	737,89 ± 21,57
11,81	38,1	25,43 ± 0,52	182,3 ± 14,31	920,19 ± 22,93

Table 4.8: Experimental Dataset collected in 2015.

Shim CR position [cm]	Reg. CR position [cm]	T [s]	Δρ [pcm]	ρ [pcm]
21,67	0	∞	0	0
21,67	9,24	33,026 ± 0,54	157,75 ± 11,22	157,75 ± 11,22
20,00	14,65	29,204 ± 0,55	169,93 ± 10,87	327,67 ± 15,62
18,00	18,92	42,065 ± 0,74	135,35 ± 8,31	463,02 ± 17,7
16,54	23,46	32,049 ± 0,78	160,67 ± 7,57	623,69 ± 19,25
14,86	28,81	31,429 ± 0,62	162,59 ± 8,48	786,29 ± 21,03
12,97	38	49,291 ± 0,6	121,82 ± 8,43	908,11 ± 22,66

Table 4.9: Experimental Dataset collected in 2018

The data in table 4.8 and 4.9 have been consequently manipulated with the least squares method in order to obtain calibration curves that will be shown in the following pages to be compared with those obtained through Serpent.

Results

The first data set was collected by students, particular, by Politecnico di Milano Nuclear Engineering students during the Experimental Nuclear Reactor Kinetics course in 2015. This dataset is characterized by the measurement of reactivity regarding eight criticality conditions and eight super criticality conditions. These configurations were simulated using the updated TRIGA Serpent model and therefore eight criticality simulations and eight super criticality simulations were performed.

Regulating Control Rod, 2015

Both the results obtained experimentally and computationally were used to reconstruct a calibration curve for the regulating control rod integral reactivity worth using the least squares method. The results obtained, along with the reconstructed integral reactivity curves are presented in figure 4.10.

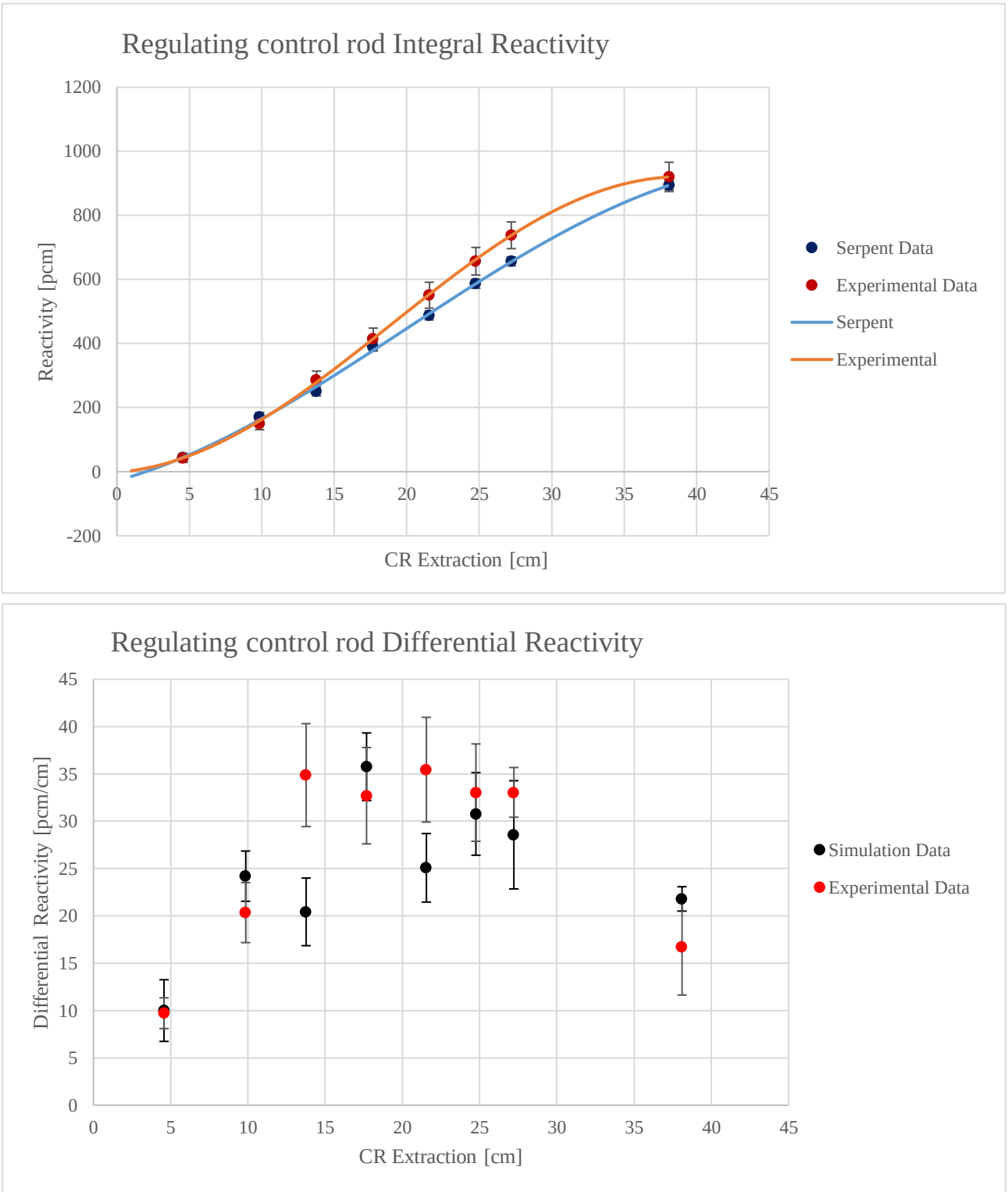

Figure 4.10: Integral (top) and differential (bottom) reactivity in pcm as a function of regulating control rod extraction in cm both for the experimental and simulated (Serpent) datasets. The year pertaining the datasets collection is 2015.

As it can be seen in figure 4.10, the simulation results and the related reconstructed curve for integral reactivity show a negative offset compared to experimental results and curve as the rod gets extracted more, but the control rod worth in terms of integral reactivity appears to be close between the two and the overall Serpent simulation results are in good agreement with experimental results; the agreement with experimental results is found within a 2σ interval considering Monte Carlo statistical uncertainty for simulation results.

The results obtained in terms of differential reactivity are shown in figure 4.10 as well and, despite a discrepancy that can be observed for two configurations, the simulation results appear in good agreement with the ones obtained through the reactor stable period method. Taking into consideration both the Monte Carlo uncertainty and the uncertainty related to the influence of systematic errors, the simulation results appear to be compatible to experimental ones within a 1σ interval. As a whole, the simulated reactivity acceptably reproduces the actual regulating control rod for what concerns the year 2015.

Shim Control Rod, 2015

In the collection of the data set, super criticality was obtained by partially extracting the regulating control rod and criticality was then restored inserting the Shim control rod. The experimental procedure went on until complete extraction of the regulating control rod was obtained. This led to the possibility of partially calibrating the shim control rod as well, assuming that the reactivity inserted at each step by the regulating control rod extraction would then be counterbalanced by the partial insertion of the shim control rod, which means that an equal in value, but negative, reactivity insertion corresponding to the preceding step was provided by shim control rod insertion at each criticality restore. The differential reactivity results obtained both experimentally and computationally are shown in figure 4.11, alongside with a reconstruction of the integral reactivity calibration curve. A good agreement between experimental and simulation data is shown here as well, even though, as already underlined, no conclusions can be drawn since there is only a partial calibration perspective.

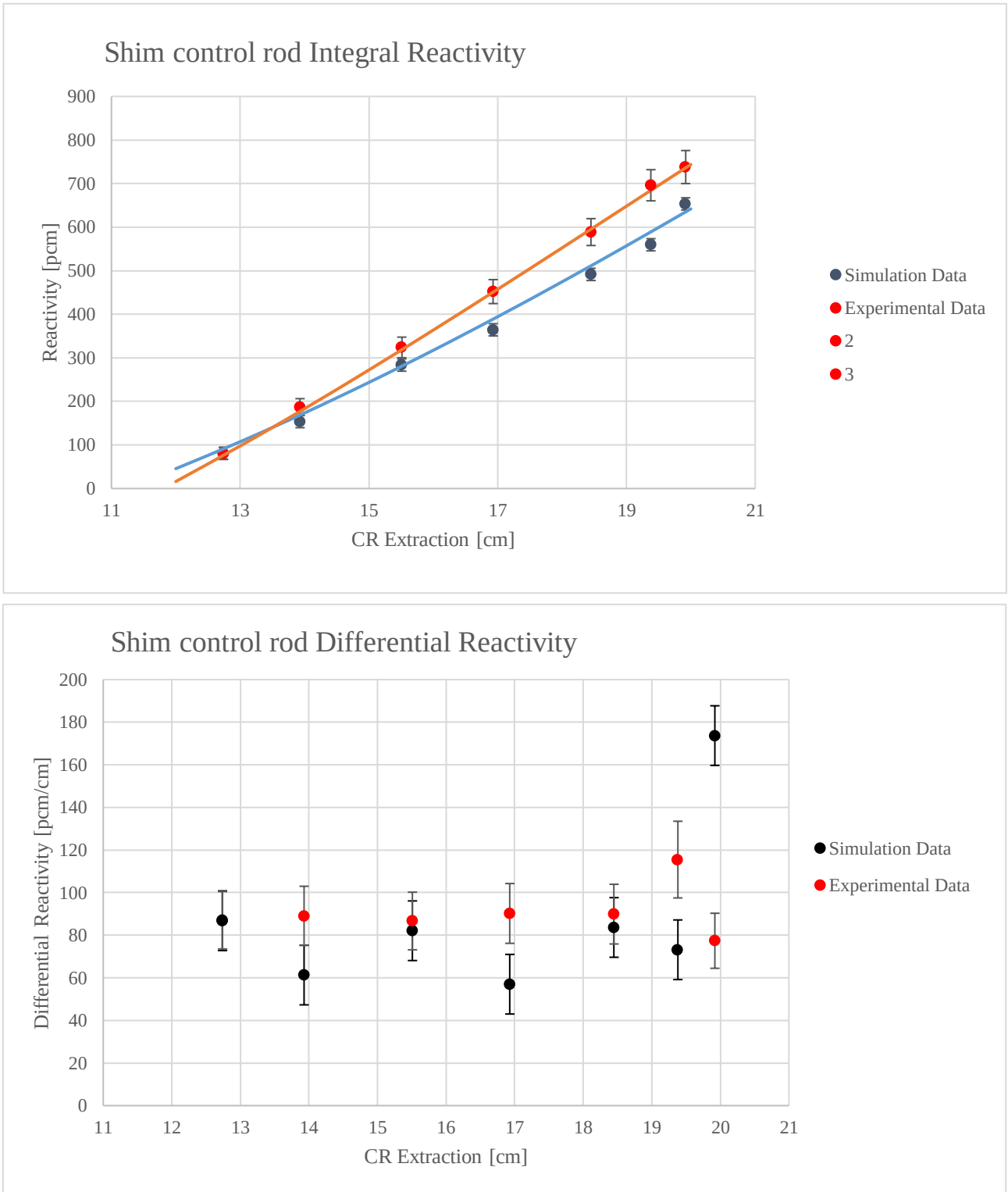

Figure 4.11: Integral (top) and differential (bottom) reactivity in pcm as a function of shim control rod extraction in cm both for the experimental and simulated (Serpent) datasets. The year pertaining the datasets collection is 2015.

A proper, even though partial, analysis for what concerns the Shim control rod can be carried out relying only on the results for what concerns differential reactivity. In fact, performing just a partial calibration, no actual data concerning integral reactivity can be exploited and the curve in figure 4.11 represents a reconstruction of the actual integral reactivity simulation for the control rod of interest. Regarding differential reactivity, it can be claimed that simulation outputs correctly reproduce experimental behavior, since even the largest discrepancies can be counterbalanced considering the uncertainties related to Monte Carlo statistics and systematic errors.

For what concerns the second data set, it was collected in the same context as the first one but in slightly different physical conditions, since, as previously mentioned, reactor operation was affected by poisons presence. In fact, the data were collected during fall 2018 and the reactor had been operated previously[16] at full power for several hours, which led to the accumulation of poisons within the reactor. This condition was taken into account when writing the input file related to these configurations and the Serpent setting for Xenon equilibrium was added to the script file. During experimental procedures, six criticality configurations and six super criticality configurations were achieved and subsequently these same twelve configurations were simulated thanks to Serpent using the updated TRIGA model. Since the model involves material definitions referring to a burnup calculation for which the reference date is September 9 2013, one would expect simulation results to have a slight higher reactivity value compared to experimental results obtained in 2018, since during five years it is fairly acceptable to assume at least a partial burnup has occurred for the materials. This was obtained, in fact, when reproducing the critical configurations shown in figure 4.4, even though they are still in good agreement with experimental reactivity within 1σ when considering the presence of systematic uncertainties, whose influence is of at least $190\ pcm$.

[16] Measurements were collected in the afternoon and the preceding operation was performed in the morning, the same day.

Regulating Control Rod, 2018

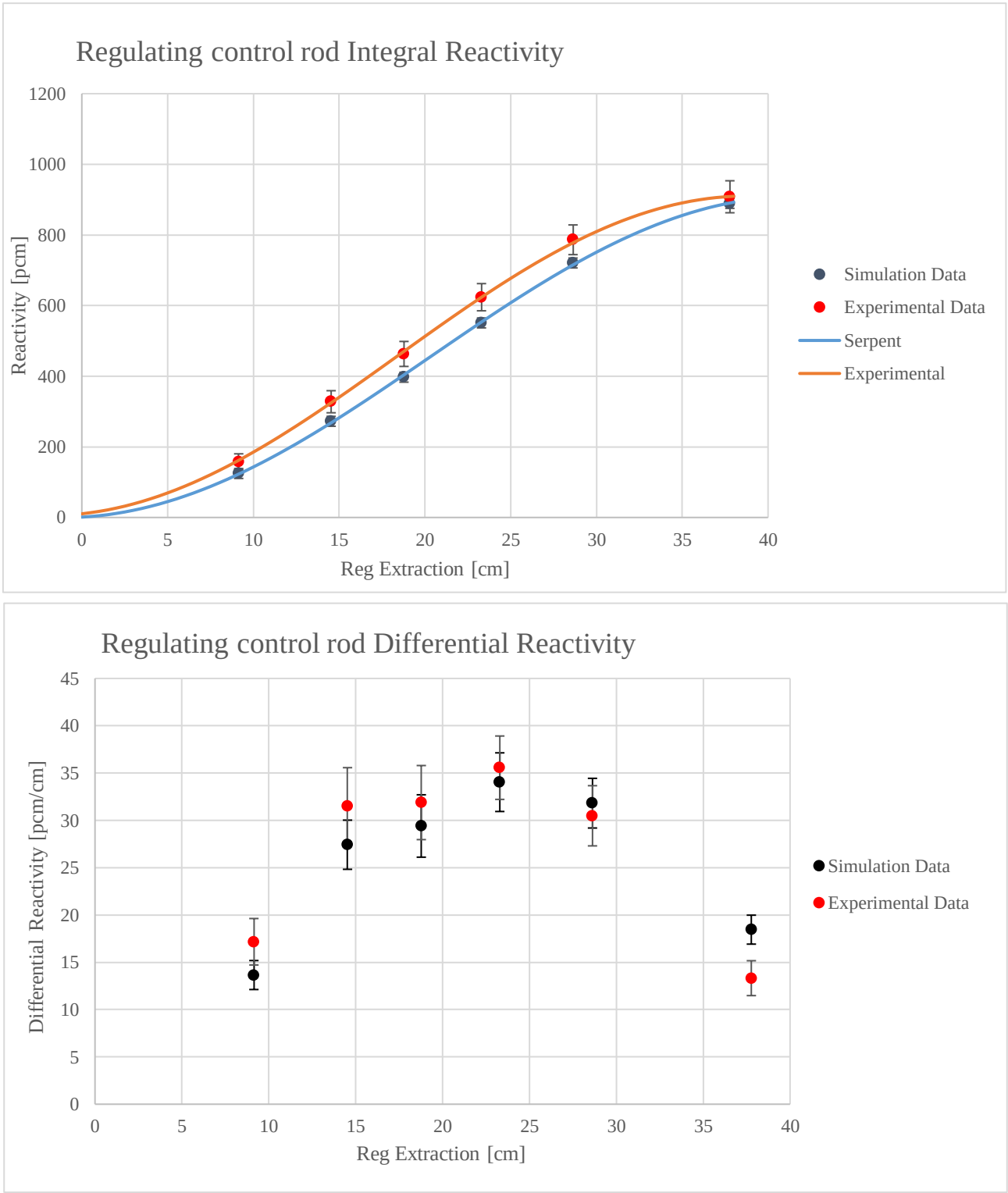

Figure 4.12: Integral (top) and differential (bottom) reactivity in pcm as a function of regulating control rod extraction in cm both for the experimental and simulated (Serpent) datasets. The year pertaining the datasets collection is 2018.

Results are still acceptable and in good agreement when referring to differential reactivity, as shown in figure 4.12. Here it can be observed that only the configuration pertaining the point in which the control rod is almost completely extracted is characterized by a simulation output which is not in perfect agreement (within 2σ, as all other differential results are) with experimental results. Differential reactivity simulated results can be inferred on average to be in good agreement with experimental results. In terms of integral reactivity, taking into consideration the whole set of uncertainties pertaining the model, the results are still acceptable in reproducing experimental reactor behavior. What has just been claimed basically means that, regarding at figure 4.12 and considering the effect of systematic errors on the results provided by Serpent, it can be said, for both integral and differential results, that simulation outputs are in good agreement with experimental data. Even so, it needs to be reminded that, as already stated, what has been obtained through Serpent simulations overestimates critical configurations in terms of reactivity compared to experimental results and this is to be linked mostly to depletion causes and might be due partially to the hypothetical insufficient Serpent precision in simulating poisons presence. The constant offset between the simulated and experimental trend for criticality configurations is to be directly related to the material definitions exploited in the model, which are not up to date when referring to the year 2018. Taking as a reference both data concerning integral and differential reactivity obtained for calibration configurations, the Serpent model is still able to faithfully predict reactor behavior from a differential point of view.

Shim Control Rod, 2018

Analogously to the dataset referred to 2015 experimental results, the partial calibration of the Shim control rod was performed in this case as well and also in this case a good agreement was found from a differential point of view.

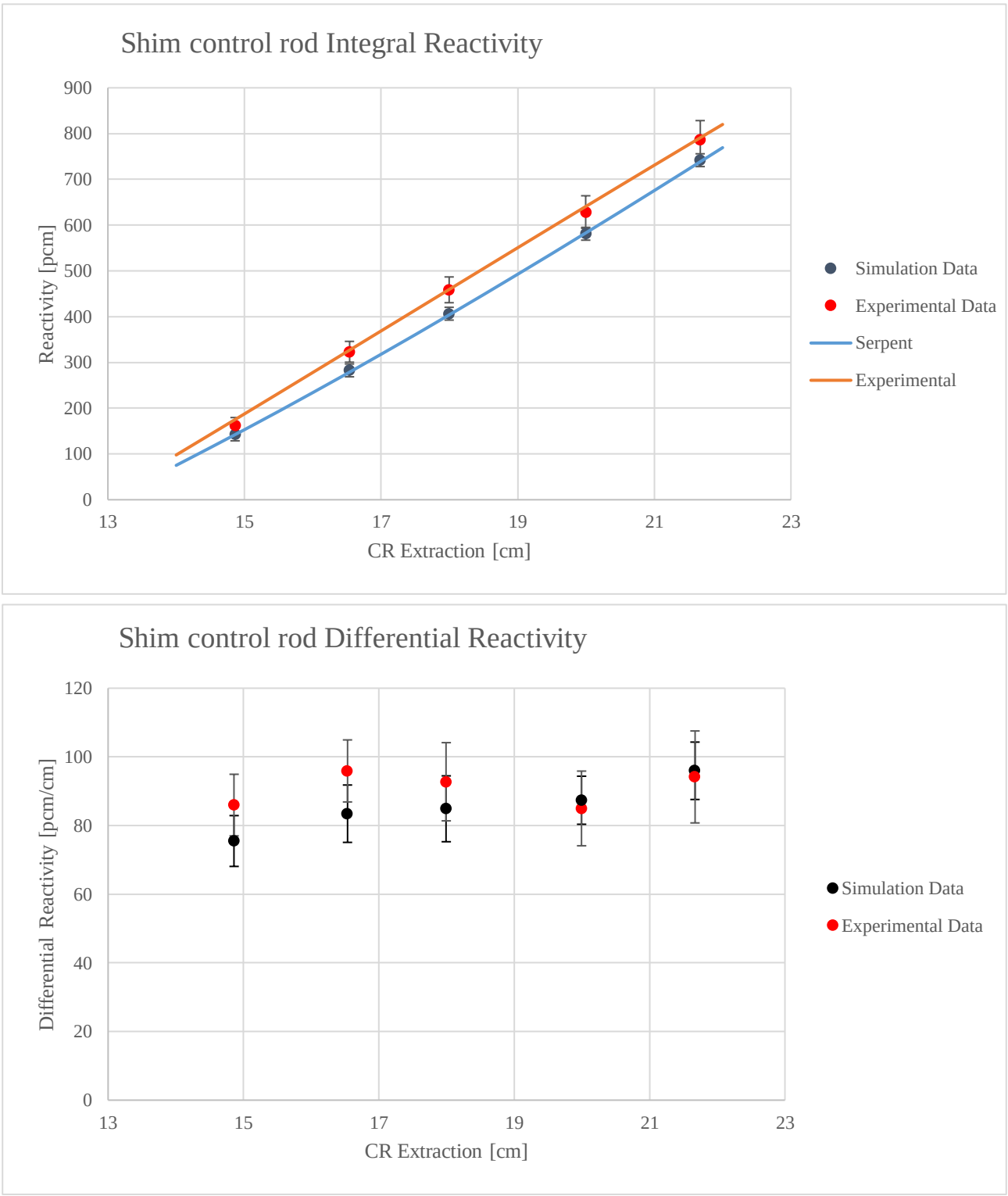

Figure 4.13: Integral (top) and differential (bottom) reactivity in pcm as a function of shim control rod extraction in cm both for the experimental and simulated (Serpent) datasets. The year pertaining the datasets collection is 2018.

For what concerns differential reactivity, the results obtained through Serpent simulations can be defined as suitable in predicting experimental results, as one can observe from figure 4.13, and this is of particular interest and significance taking into consideration the fact that the shim control rod is the one responsible of coarse reactivity variations. For what concerns integral reactivity, it is to be specified once again that, in both cases, the data collected for the shim control rod were not sufficient to perform a complete calibration, which means that the curves related to integral reactivity are a very rough approximated reconstruction of the integral reactivity trend of the shim control rod. Regarding the results obtained for differential reactivity, the agreement between simulated and experimental data can be observed and it is within a 2σ interval.

Considering as a whole the data pertaining all calibrations for all the rods in the two datasets, an agreement within the uncertainty sources considered in the analysis can be found between experimental data and the output data provided by Serpent simulations. Even though discrepancies can be found for what concerns reactivity for criticality configurations of the year 2018 and they can be linked to burnup-related phenomena, it can be inferred that the model developed for the TRIGA Mark II reactor is a valid instrument for reactor analysis.

χ^2 Test

In order to analyze thoroughly the results provided by the model, a χ^2 test was performed (Taylor, 1997) comparing the values pertaining the calibration of the regulating and shim control rods obtained via Serpent and experimentally. This procedure was carried out on differential reactivity results both for the 2015 and 2018 datasets. The basic concept behind the use of the χ^2 test for the purpose of interest lays is computing the following:

$$\chi^2 = \sum_{i=1}^{N} \left(\frac{x_i - \mu_i}{\sigma_i} \right)^2$$

It is useful to point out the meaning of the quantities that are part of the above expression. N is the number of samples considered, which in the case of interest is the number of values for differential reactivity in the datasets, while x_i and μ_i are the differential reactivity values obtained respectively via simulation and experimentally for the i-th calibration point. The quantity σ_i represents the combined uncertainty for the sample, considering both the experimental and Monte Carlo uncertainties, for the i-th calibration point. The expected value for the quantity χ^2 is the number corresponding to the so called *degrees of freedom* ν, which in this case is equal to N. The goodness of the simulation output can be inferred measuring the discrepancy between the value obtained for $\chi^2$and ν: the closer the two, the more precise the simulation result. For less accurate model outputs, the discrepancy between the values increases, in particular:

$$\chi^2 \gg \nu$$

The *p-value* for each case was computed as well; it represents the probability of obtaining a χ^2 value equal or greater than the one that was actually obtained. The significance level for such a parameter was taken as 5 %. This means that obtaining a value greater than 5% confirms a rather good agreement between experimental and simulated data.

As previously claimed, this test was performed for both the regulating and shim control rods, based of differential reactivity results, which are independent samples. The results, along with the values for ν are presented in table 4.14 and 4.15.

Control Rod	χ^2	ν	p-value
Regulating	13,16	8	10%
Shim	17,03	7	1,9%

Table 4.14: Results for the χ^2 test for the regulating and control rods for the 2015 dataset.

Control Rod	χ^2	ν	p-value
Regulating	7,21	6	30%
Shim	5,35	5	40%

Table 4.15: Results for the χ^2 test for the regulating and control rods for the 2018 dataset

From both table 4.14 and 4.15 it can be inferred that the simulation results are overall in good agreement with experimental results, and a slight better reproduction in terms of differential reactivity can be observed from the 2018 dataset, which is not directly noticeable from the plots shown previously. The only p-value that resulted in being below 5% is the one of the 2015 data for the Shim control rod. For this particular dataset, it can be seen in figure 4.11 that the position in which the Shim control rod is most extracted corresponds to a rather high discrepancy between experimental and simulated outputs, compared to other results. This particular datum could have had a significant impact on the obtained χ^2 value. It is important to underline the role of systematic uncertainties in influencing simulation results, providing offsets and shifting outputs in terms of reactivity values, as already mentioned. These results are a further validation of what already stated, which is that the updated model is suitable for predicting reactivity behavior, overall in differential terms, for both experimental datasets from 2015 and 2018.

Regarding the results obtained as a whole, it is possible to say that the model update faithfully represents reactor conditions at the time of the core reconfiguration for what concerns both low power and full power conditions. The regulating control rod calibration and the shim control rod partial calibration can be achieved via Serpent simulations and results obtained are in good agreement for what concerns both integral and differential reactivity when considering experimental procedures performed in a time frame close to the core reconfiguration, while for procedures

performed after a longer[17] time has passed, material burnup calculations should be performed in order to obtain more reliable criticality reactivity results, while the differential and calibration ones still hold.

It is important to underline that full compatibility has been found between all the results analyzed within a 2σ interval, considering sources of uncertainty for the simulation outputs which are the ones related to the Monte Carlo intrinsic statistical error ($7\ pcm$ for all simulations that were performed) and to systematic errors (at least $190\ pcm$ for the TRIGA Mark II reactor of the University of Pavia). An additional burnup analysis would be useful in order to achieve a higher level of accuracy in determining simulation outputs in terms of more adherence to actual reactor criticality when performing a benchmark analysis with experimental results.

[17] As an estimate, the minimum time frame is between two and five years.

Conclusion

This thesis work has been developed with the aim of developing a model for the current configuration of the TRIGA Mark II reactor of the University of Pavia. exploiting the Monte Carlo neutron transport code Serpent 2. The basis for this work was a preceding model for the same reactor, developed with Serpent 1 studying its condition as it was when its first operation took place in 1965. Since during the years the core configuration and other details pertaining the reactor changed, the model built upon the 1965 configuration would not serve as a close representative of today's reactor conditions and the model had to be adjusted. The fresh fuel model developed was initially tested with Serpent 2 and criticality configurations were reproduced correctly. In order to update the model, the available public data concerning the reactor both from a geometry and material point of view were exploited. In particular, burnup calculation results pertaining fuel elements were adopted to correctly represent material conditions as in September 2013, together with the new core configuration achieved in the same time frame. These two sets of information were implemented in Serpent 2 input scripts and the model was updated to September 2013 reactor state. The model was validated and results both for the first full power criticality and for the core excess resulted in being acceptable compared to experimental values. In particular, the results obtained reproducing the first full power criticality condition with Serpent 2 were satisfactory since a reactivity value of about $2\ pcm$ was obtained. This result is in fact in good agreement with experimental benchmarks, taking into consideration the uncertainty featuring simulation results. The model was then exploited to calibrate the regulating control rod and to partially calibrate the shim

control rod as well, taking as a reference for comparison two data sets, one collected in 2015 and the second one collected in 2018, for which reactivity was measured using the reactor stable period method. While the simulation results related to the 2015 dataset showed good agreement both in terms of differential and integral reactivity trends and values, the ones referring to the 2018 dataset were characterized by an offset towards higher reactivity values when reproducing criticality configurations. What was actually found was a good agreement with experimental data when considering reactivity in terms of calibration points and curves, considering a 2σ interval comprehensive of all sources of uncertainty around simulations outputs. It needs to be underlined that, considering uncertainty sources such as those related to statistics and systematic errors, most reactivity values obtained for 2018 criticality simulated configurations eventually show a good agreement with experimental criticalities. Despite what just stated, the main reason for the offset can be linked to different causes, but most of all to the fact that simulations refer to a reactor condition that is five years prior to the 2018 dataset experimental procedure and thus materials within the reactor have undergone burnup processes during those five years. It is therefore possible to assert that the Serpent model was acceptably adapted to the conditions referring to 2013 and experimental data up to the year 2015 can still be simulated with acceptable accuracy. For what concerns time frames longer than a two-year period, criticality configurations show an offset towards higher reactivities that is still within acceptable limits coming from systematic and Monte Carlo error intervals; a further development might exploit some burnup calculations in order to try and obtain simulation results which better reflect criticality configurations pertaining this time frame. Results in terms of differential and integral reactivity when performing a control rod calibration, for the year 2018, appear to still be acceptable, taking into consideration all the uncertainty sources for the specific reactor and simulation tool. It can be therefore claimed that the updated model developed for the TRIGA Mark II reactor of the University of Pavia correctly and validly reproduces reactor behavior and can be exploited as a useful reactor analysis tool. Future applications might include its involvement in burnup calculations and coupling with

thermal-hydraulic codes for a more thorough description of the TRIGA Mark II reactor.

Bibliography

Alloni, D., di Tigliole, A. B., Cammi, A., Chiesa, D., Clemenza, M., Magrotti, G., Pattavina, L., Pozzi, S., Prata, M. and Previtali, E. (2014) 'Final characterization of the first critical configuration for the TRIGA Mark II reactor of the University of Pavia using the Monte Carlo code MCNP', *Progress in Nuclear Energy*, 74, pp. 129-135.

Briesmeister, J. F. (1986) 'MCNP-A general Monte Carlo code for neutron and photon transport', *LA-7396-M*.

Brown, F. B. (2006) 'The makxsf code with Doppler Broadening', *Los Alamos National Laboratory. LA-UR-06-7002*.

Cambieri, A., Cingoli, F., Meloni, S. and Orvini, E. (1965) *Il reattore TRIGA Mark II da 250 kW, pulsato, dell'Universita di Pavia. Rapporto finale sulle prove nucleari*: Internal Report.

Cammi, A., Di Marcello, V., Luzzi, L. and Memoli, V. (2011) 'The multi-physics modelling approach oriented to safety analysis of innovative nuclear reactors', *Advances in Energy Research*, 5, pp. 171-214.

Cammi, A., Zanetti, M., Chiesa, D., Clemenza, M., Pozzi, S., Previtali, E., Sisti, M., Magrotti, G., Prata, M. and Salvini, A. (2016) 'Characterization of the TRIGA Mark II reactor full-power steady state', *Nuclear Engineering and Design*, 300, pp. 308-321.

Castagna, C., Chiesa, D., Cammi, A., Boarin, S., Previtali, E., Sisti, M., Nastasi, M., Salvini, A., Magrotti, G. and Prata, M. (2018) 'A new model with Serpent for the first criticality benchmarks of the TRIGA Mark II reactor', *Annals of Nuclear Energy*, 113, pp. 171-176.

Chadwick, M. B., Herman, M., Obložinský, P., Dunn, M. E., Danon, Y., Kahler, A. C., Smith, D. L., Pritychenko, B., Arbanas, G. and Arcilla, R. (2011) 'ENDF/B-VII. 1 nuclear data for science and technology: cross sections, covariances, fission product yields and decay data', *Nuclear data sheets*, 112(12), pp. 2887-2996.

Chiesa, D. (2014) 'Development and experimental validation of a Monte Carlo simulation model for the Triga Mark II reactor'.

Chiesa, D., Clemenza, M., Pozzi, S., Previtali, E., Sisti, M., Alloni, D., Magrotti, G., Manera, S., Prata, M., Salvini, A., Cammi, A., Zanetti, M. and Sartori, A. (2016) 'Fuel burnup analysis of the TRIGA Mark II reactor at the University of Pavia', *Annals of Nuclear Energy,* 96, pp. 270-276.

Duderstadt, J. J. and Hamilton, L. J. 'Nuclear reactor analysis. 1976', *Ann Arbor, Michigan: Wiley-Interscience,* 650.

Lamarsh, J. R. (1966) *Nuclear Reactor Theory.* Addison-Wesley.

Leppänen, J. (2007) *Development of a new Monte Carlo reactor physics code.* VTT Technical Research Centre of Finland.

Leppänen, J. (2013) 'Serpent–a continuous-energy Monte Carlo reactor physics burnup calculation code', *VTT Technical Research Centre of Finland,* 4.

Leppänen, J., Pusa, M., Viitanen, T., Valtavirta, V. and Kaltiaisenaho, T. 'The Serpent Monte Carlo code: Status, development and applications in 2013'. 2014: EDP Sciences, 06021.

Metropolis, N. and Ulam, S. (1949) 'The monte carlo method', *Journal of the American statistical association,* 44(247), pp. 335-341.

Moffat, R. J. (1988) 'Describing the uncertainties in experimental results', *Experimental thermal and fluid science,* 1(1), pp. 3-17.

Santamarina, A., Bernard, D., Blaise, P., Coste, M., Courcelle, A., Huynh, T. D., Jouanne, C., Leconte, P., Litaize, O. and Mengelle, S. (2009) 'The JEFF-3.1. 1 nuclear data library', *JEFF report,* 22(10.2), pp. 2.

Taylor, J. (1997) *Introduction to error analysis, the study of uncertainties in physical measurements.*

Team, X. M. C. 2003. MCNP—A General Monte Carlo N-Particle Transport Code, Version 5. Los Alamos National Laboratory Los Alamos, NM.